

# Geometric and Electronic Structures of Phenoxyl Radicals Hydrogen Bonded to Neutral and Cationic Partners

Maylis Orio,<sup>[a]</sup> Olivier Jarjayes,<sup>[b]</sup> Benoit Baptiste,<sup>[b]</sup> Christian Philouze,<sup>[b]</sup>  
Carole Duboc,<sup>[c]</sup> Jenny-Lee Mathias,<sup>[d]</sup> Laurent Benisvy,<sup>\*[d]</sup> and Fabrice Thomas<sup>\*[b]</sup>

**Abstract:** Two di-*tert*-butylphenols incorporating an *N*-methylbenzimidazole moiety in the *ortho* or *para* position have been synthesised (<sup>Me</sup>OH and <sup>pMe</sup>OH, respectively). Their X-ray structures evidence a hydrogen bond between the phenolic proton and the iminic nitrogen atom, whose nature is intra- and intermolecular, respectively. The present studies demonstrate that <sup>Me</sup>OH is readily oxidised by an intramolecular PET mechanism to form the hydrogen-bonded phenoxyl-*N*-methylbenzimidazolium system (<sup>Me</sup>OH)<sup>•+</sup>, whereas oxidation of <sup>pMe</sup>OH occurs by intermolecular PET, affording the neutral phenoxyl benzimidazole (<sup>pMe</sup>O)<sup>•</sup> system. The deprotonations of <sup>Me</sup>OH

and <sup>pMe</sup>OH yield the corresponding phenolate species (<sup>Me</sup>O)<sup>−</sup> and (<sup>pMe</sup>O)<sup>−</sup>, respectively, whilst that of the previously reported <sup>H</sup>OH (analogous to <sup>Me</sup>OH but lacking the *N*-methyl group) produces an unprecedented hydrogen-bonded phenol benzimidazolate species, as evidenced by its X-ray structure. The latter is believed to be in equilibrium in solution with its tautomeric phenolate form, as suggested by NMR, electrochemistry and DFT stud-

**Keywords:** density functional calculations • electronic structure • electron transfer • hydrogen bonds • phenoxyl radicals

ies. The one-electron oxidations of the anions occur by a simple ET process affording phenoxyl radical species, whose electronic structure has been studied by HF-EPR spectroscopy and DFT calculations. In particular, analysis of the *g*<sub>1</sub> tensor shows the order 2.0079 > 2.0072 > 2.0069 > 2.0067 for (<sup>Me</sup>O)<sup>•</sup>, (<sup>H</sup>O)<sup>•</sup>, (<sup>Me</sup>OH)<sup>•+</sup> and (<sup>H</sup>OH)<sup>•+</sup>, respectively. (<sup>Me</sup>O)<sup>•</sup> exhibits the largest *g*<sub>1</sub> tensor (2.0079), consistent with the absence of intramolecular hydrogen bond. The *g*<sub>1</sub> tensor of (<sup>H</sup>O)<sup>•</sup> is intermediate between those of (<sup>Me</sup>OH)<sup>•+</sup> and (<sup>Me</sup>O)<sup>•</sup> (*g*<sub>1</sub> = 2.0072), indicating that the phenoxyl oxygen is hydrogen-bonded with a neutral benzimidazole partner.

## Introduction

Tyrosyl radicals are of widespread importance in biological systems, since they are involved in many enzymatic processes.<sup>[1–7]</sup> A prototypical example of a tyrosyl radical protein is the water-oxidising photosystem II (PSII), in which Tyr<sub>Z</sub><sup>•</sup> acts as a relay in the transfer of electrons between the P680 chlorophylls and the water-oxidising manganese cluster, as well as being directly potent in water oxidation through H-atom abstraction.<sup>[1–3]</sup> Interestingly, PSII contains a second tyrosyl radical, namely, Tyr<sub>D</sub><sup>•</sup>, which has been found to be more stable than Tyr<sub>Z</sub><sup>•</sup>. The biological function of Tyr<sub>D</sub><sup>•</sup> is unknown, but it has clearly been shown that Tyr<sub>D</sub><sup>•</sup> is not involved in water oxidation in PSII during photosynthesis. Another example of importance is galactose oxidase, in which the tyrosyl radical is coordinated to a Cu<sup>II</sup> ion.<sup>[4]</sup> It is directly involved in catalysis by abstracting an H atom from the alcohol substrate. Among the other enzymes which are believed to generate tyrosyl radicals on their own peptidic chain, the best known are ribonucleotide reductase,<sup>[1,5]</sup> cytochrome c oxidase<sup>[1,6]</sup> and prostaglandin H synthase.<sup>[1,7]</sup> Modulation of tyrosyl radical formation and its reactivity is believed to be achieved through metal coordination (if applicable) or the existence of hydrogen bonds with a neighbouring base (e.g., His). During the last few years chemical models for hydrogen-bonded tyrosyl radicals have been

- [a] Dr. M. Orio  
Laboratoire de Spectrochimie Infrarouge et Raman  
Bâtiment C5 - UMR CNRS 8516  
Université des Sciences et Technologies de Lille  
59655 Villeneuve d'Ascq Cedex (France)
- [b] Dr. O. Jarjayes, Dr. B. Baptiste, Dr. C. Philouze, Prof. Dr. F. Thomas  
Département de Chimie Moléculaire  
Chimie Inorganique Redox Biomimétique (CIRE)  
UMR-5250, Université Joseph Fourier  
BP 53, 38041 Grenoble Cedex 9 (France)  
Fax: (+33) 476-51-4836  
E-mail: Fabrice.Thomas@ujf-grenoble.fr
- [c] Dr. C. Duboc  
Laboratoire National des Champs Magnétiques Intenses (LCNMI)  
UPR CNRS 3228, BP 166, 38042 Grenoble Cedex 9 (France)  
Present address: Département de Chimie Moléculaire  
Chimie Inorganique Redox Biomimétique (CIRE), UMR-5250  
Université Joseph Fourier  
BP 53, 38041 Grenoble Cedex 9 (France)
- [d] J.-L. Mathias, Dr. L. Benisvy  
Laboratory of Biomimetic Chemistry  
Department of Chemistry, Bar-Ilan University  
Ramat Gan 52900 (Israel)  
Fax: (+972) 3-7384053  
E-mail: benisvl@mail.biu.ac.il

Supporting information for this article is available on the WWW under <http://dx.doi.org/10.1002/chem.201102854>.

characterised.<sup>[8–17]</sup> Evidence has then been gathered that oxidation of tyrosine, if not coordinated to a metal ion, occurs by a proton-coupled electron-transfer (PET) mechanism.<sup>[18]</sup> Indeed, the oxidation potential of tyrosine (TyrOH<sup>•+</sup>/TyrOH couple) is high (1.4 to 1.5 V vs. NHE in water),<sup>[18]</sup> and is not compatible with the fact that enzymes operate with small reaction free energies. Recent electrochemical and kinetic investigations performed on phenolic compounds that are intramolecularly hydrogen-bonded to an adjacent base (e.g. imidazole, pyridine) have revealed that coupling of the oxidation reaction with proton-electron transfer (PET) improves the driving force of the reaction.<sup>[11,18]</sup> In addition, the oxidation process is concerted (CPET) in order to avoid unfavourable formation of charges during the reaction. “Concerted” in this case implies that both the electron and the proton move in a single kinetic step.<sup>[11]</sup>

One of the most powerful techniques to probe the local environment of tyrosyl radicals in proteins is high-field EPR (HF-EPR), which allows for determination of the *g*-tensor anisotropy and thus the three principal *g* values.<sup>[3]</sup> More specifically, an electropositive environment like the presence of a hydrogen bond induces a shift of the low-field component *g*<sub>1</sub> that can be experimentally detected in enzymatic systems. We recently reproduced the lowering of *g*<sub>1</sub> as a result of hydrogen-bonding interaction between the phenoxyl oxygen atom and a cationic partner in biomimetic models.<sup>[10,17]</sup> To date the effect of the charge of the donor on the *g* tensor in hydrogen-bonded phenoxyl radicals has been poorly documented, although it is of major importance for characterising intermediates and better understanding biological processes that involve tyrosyl radical species (Figure 1).<sup>[18–19]</sup> It has been previously shown by combined spectroscopic and theoretical methods that oxidation of phenol-imine conjugates,<sup>[9–12]</sup> and especially <sup>H</sup>OH (Figure 2),<sup>[10]</sup> occurs by an intramolecular PET mechanism, affording a phenoxyl radical hydrogen-bonded to an iminium cationic partner. Detailed

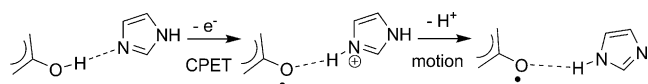


Figure 1. Proposed mechanism for the formation of the stable Tyr<sub>D</sub><sup>•</sup> radical in photosystem II.

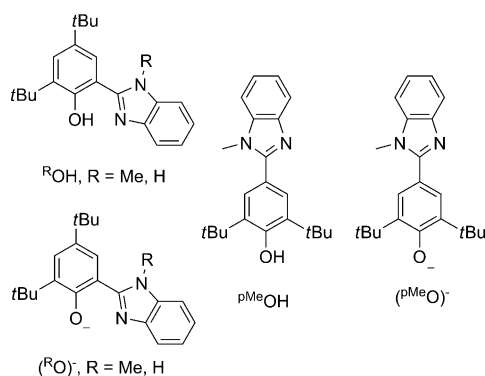


Figure 2. Compounds of interest in this study.

thermodynamic and kinetic investigations on <sup>H</sup>OH have provided additional important insights into the redox mechanism<sup>[12]</sup> and have elegantly shown that such compounds are among the best models of the Tyr<sub>2</sub>-His pair of PSII.<sup>[10–12,15]</sup>

In an effort to better understand the parameters that influence the electronic structure and the *g*-tensor anisotropy of hydrogen-bonded phenoxyl radicals we herein complement our previous works by investigating the effect of the charge of the partner. Because of their relatively high stability we investigate phenol-benzimidazole compounds<sup>[10]</sup> rather than Mannich bases.<sup>[17]</sup> With the aim of tuning the charge of the hydrogen-bond partner (benzimidazole group) and controlling the mechanism of radical formation (CPET or ET), we herein extend the electrochemical, spectroscopic and theoretical studies that we performed on <sup>H</sup>OH<sup>[10]</sup> to the deprotonated derivative (<sup>H</sup>O)<sup>•−</sup><sup>[16]</sup> (Figure 2). In addition, we introduce the new *N*-methylated phenol <sup>Me</sup>OH and its corresponding phenolate (<sup>Me</sup>O)<sup>•−</sup> (Figure 2) in order to gain insight on the effect of hydrogen-bonding on the properties of the corresponding phenoxyl radicals.

To discriminate the effect of delocalisation from pure electrostatic effects, we introduce the new compound <sup>pMe</sup>OH and phenolate (<sup>pMe</sup>O)<sup>•−</sup>, which have an *N*-methylbenzimidazole group connected to the phenol group at the *para* position, and thus are unable to establish an intramolecular hydrogen bond between the phenolic proton and the *N*-methylbenzimidazole.

We herein demonstrate that phenoxyl radical properties (i.e., oxidation potential, electronic structure and their *g* tensors) are subtly modulated by the charge of the hydrogen-bonded partner, the strength of the hydrogen-bonding interaction and their deviation from planarity.

## Results and Discussion

Phenolic compounds <sup>H</sup>OH, <sup>Me</sup>OH and <sup>pMe</sup>OH were synthesised in one step, as described in the Experimental Section. The corresponding phenolates (<sup>H</sup>O)<sup>•−</sup>, (<sup>Me</sup>O)<sup>•−</sup> and (<sup>pMe</sup>O)<sup>•−</sup> were synthesised by treating the parent phenol with a stoichiometric amount of base *n*Bu<sub>4</sub>NOH, isolated and characterised (see Experimental Section).

**X-ray crystal structures of <sup>H</sup>OH, <sup>Me</sup>OH, <sup>pMe</sup>OH, (<sup>Me</sup>O)<sup>•−</sup> and (<sup>H</sup>O)<sup>•−</sup>:** The X-ray crystal structure of <sup>H</sup>OH·0.5H<sub>2</sub>O has been reported previously.<sup>[10]</sup> Herein we describe briefly a new unsolvated structure for this compound and present in details the structures of unprecedented <sup>Me</sup>OH, <sup>pMe</sup>OH, (<sup>Me</sup>O)<sup>•−</sup> and (<sup>H</sup>O)<sup>•−</sup> (Figure 3, Table 1).

In unsolvated <sup>H</sup>OH the iminic nitrogen atom N1 is involved in a bifurcated hydrogen-bond network. One is intramolecular with phenolic hydrogen atom H1 (O1...N1 2.74 Å and ∠OH...N 149°), while the other is intermolecular with the amino nitrogen atom N2 of another molecule (N1...H26'–N2' 2.99 Å), leading to the formation of polymeric chains (see Supporting Information). In contrast to the structure of <sup>H</sup>OH·0.5H<sub>2</sub>O, in which the three independ-

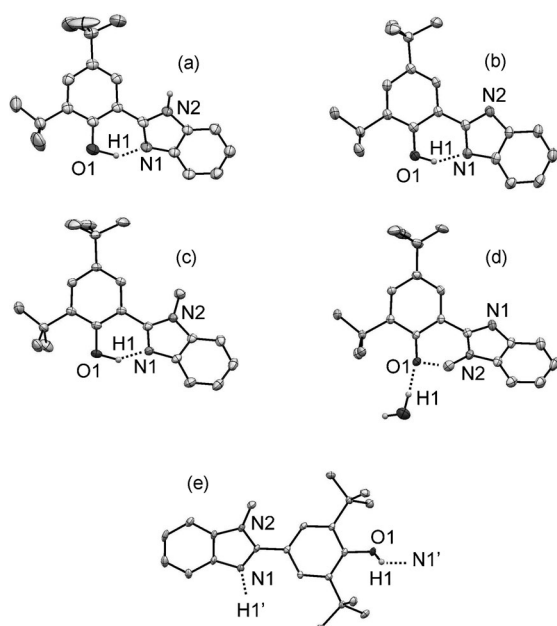


Figure 3. ORTEP diagrams of the molecular structures of a)  $\text{H}_2\text{OH}$ , b)  $(\text{H}_2\text{O})^-$  in  $(\text{H}_2\text{O})[\text{nBu}_4\text{N}]\cdot\text{H}_2\text{O}$ , c)  $\text{MeOH}$ , d)  $(\text{MeO})^- \cdot \text{H}_2\text{O}$  in  $(\text{MeO})^-[\text{nBu}_4\text{N}]\cdot 2.4\text{H}_2\text{O}$ , and e)  $\text{pMeOH}$  shown with 30% thermal ellipsoids. Hydrogen atoms are omitted for clarity except the phenolic and amino ones.

ent molecules appear to be quasi-planar (phenol/imidazole twist angles of  $7\text{--}17^\circ$ ),<sup>[10]</sup> the new unsolvated  $\text{H}_2\text{OH}$  structure deviates significantly from planarity with a phenol/imidazole twist angle of  $29^\circ$ . This polymorphism thus suggests that solid-state structures should be used with special care when estimating the strength of the hydrogen bond between phenol protons and imino acceptor, as recently emphasised by Mayer et al.<sup>[12]</sup>

The crystal structure of  $\text{MeOH}$  (Figure 3c) shows that the phenol and *N*-methylbenzimidazole rings are not coplanar, but twisted by  $33^\circ$ . This deviation from planarity is most likely due to a steric clash between the *N*-methyl group and one of the *meta*-H atoms of the phenol group. Yet, stabilising intramolecular hydrogen-bonding between the phenolic hydrogen atom and the *N*-methylbenzimidazole iminic nitrogen atom is established, as evidenced by the short  $\text{O1}\cdots\text{N1}$  distance ( $2.65\text{ \AA}$ ), and the  $\text{O1-H1}\cdots\text{N1}$  angle of  $150^\circ$ . Interestingly, the  $\text{C1-O1}$  bond length of  $1.366(2)\text{ \AA}$  is consistent with a phenol and resembles that of  $\text{H}_2\text{OH}$  ( $1.367(3)\text{ \AA}$ ). The structure of  $\text{pMeOH}$  is shown in Figure 3e. The phenol and *N*-methylbenzimidazole rings are twisted by  $42^\circ$ . In addition, the  $\text{C1-O1}$  bond length ( $1.361(3)\text{ \AA}$ ) is similar to those of  $\text{MeOH}$  and  $\text{H}_2\text{OH}$ . An intermolecular hydrogen bond exists between phenolic hydrogen atom H1 and the *N*-methylbenzimidazole iminic nitrogen atom N1' of another molecule, as judged by the  $\text{O1}\cdots\text{N1'}$  distance of  $2.91\text{ \AA}$  and the  $\text{O1-H1}\cdots\text{N1'}$  angle of  $154^\circ$ .

The corresponding anions  $(\text{H}_2\text{O})^-$  and  $(\text{MeO})^-$  have both been structurally characterised as tetrabutylammonium salts (Figure 3b,d). Both X-ray structures contain water molecules ( $[\text{H}_2\text{O}][\text{nBu}_4\text{N}]\cdot\text{H}_2\text{O}$  and  $[\text{MeO}][\text{nBu}_4\text{N}]\cdot 2.4\text{H}_2\text{O}$ ), which establish intermolecular hydrogen bonds with imidazole N acceptors to form dimers  $\{\text{H}_2\text{O}\cdots\text{H}_2\text{O}\cdots\text{H}_2\text{O}\cdots\text{O}^-\}$  in the former or with both phenolate  $\text{O}^-$  and imidazole N acceptors yielding a linear polymer chain  $\{\text{MeO}\cdots\text{H}_2\text{O}\cdots\text{H}_2\text{O}\cdots\text{O}^-\}_n$  in the latter salt (see Supporting Information).

The structure of  $(\text{MeO})^-$  differs significantly from that of its corresponding phenol parent  $\text{MeOH}$ . Indeed, the *N*-Me group is now pointing toward the phenolate  $\text{O}^-$  atom (phenol/imidazole twist angle ca.  $139^\circ$ ), whereas in  $\text{MeOH}$  it points in the opposite direction (see Figure 3c, d).

Table 1. Crystallographic data for  $\text{H}_2\text{OH}$ ,  $(\text{H}_2\text{O})[\text{nBu}_4\text{N}]\cdot\text{H}_2\text{O}$ ,  $\text{MeOH}$ ,  $(\text{MeO})[\text{nBu}_4\text{N}]\cdot 2.4\text{H}_2\text{O}$ , and  $\text{pMeOH}$ .

	$\text{H}_2\text{OH}$	$(\text{H}_2\text{O})[\text{nBu}_4\text{N}]\cdot\text{H}_2\text{O}$	$\text{MeOH}$	$(\text{MeO})[\text{nBu}_4\text{N}]\cdot 2.4\text{H}_2\text{O}$	$\text{HLpMe}$
formula	$\text{C}_{21}\text{H}_{26}\text{N}_2\text{O}$	$\text{C}_{37}\text{H}_{43}\text{N}_3\text{O}_2$	$\text{C}_{22}\text{H}_{28}\text{N}_2\text{O}$	$\text{C}_{38}\text{H}_{67.8}\text{N}_3\text{O}_{3.4}$	$\text{C}_{22}\text{H}_{28}\text{N}_2\text{O}$
<i>M</i>	322.45	581.92	336.48	621.17	336.46
crystal system	monoclinic	monoclinic	monoclinic	monoclinic	monoclinic
space group	$P2_1/a$	$P2_1/c$	$P2_1/n$	$P2_1/c$	$P12_1/c1$
<i>a</i> [ $\text{\AA}$ ]	10.145(7)	16.153(5)	6.085(2)	14.02(1)	15.449(7)
<i>b</i> [ $\text{\AA}$ ]	11.854(3)	32.515(9)	36.08(7)	24.70(1)	9.911(2)
<i>c</i> [ $\text{\AA}$ ]	15.930(3)	19.087(4)	9.225(1)	16.65(1)	12.052(6)
$\alpha$ [ $^\circ$ ]	90	90	90	90	90
$\beta$ [ $^\circ$ ]	91.96(3)	132.69(2)	103.05(3)	137.77(3)	92.44(5)
$\gamma$ [ $^\circ$ ]	90	90	90	90	90
<i>V</i> [ $\text{\AA}^3$ ]	1915(1)	7369(4)	1973(1)	3875(4)	1843.8(13)
<i>Z</i>	4	8	4	4	4
<i>T</i> [K]	293	200	293	200	200
$\rho_{\text{calcd}}$ [ $\text{g cm}^{-3}$ ]	1.180	1.049	1.133	1.065	1.212
$\mu$ [ $\text{cm}^{-1}$ ]	0.534	0.064	0.069	0.067	0.74
monochromator	graphite	graphite	graphite	graphite	graphite
radiation	$\text{Cu K}\alpha$	$\text{Mo K}\alpha$	$\text{Mo K}\alpha$	$\text{Mo K}\alpha$	$\text{Mo K}\alpha$
$\lambda$ [ $\text{\AA}$ ]	1.5418	0.71073	0.71073	0.71073	0.71073
reflns collected	4278	55 699	23 012	30 003	3202
independent reflns ( $R_{\text{int}}$ )	4248 (0.09616)	12 816 (0.09642)	3496 (0.11680)	6935 (0.15944)	2228 (0.1225)
observed reflns	2522 [ $I > 2\sigma(I)$ ]	8423 [ $I > 2\sigma(I)$ ]	2138 [ $I > 2\sigma(I)$ ]	4268	3202 [ $I > 2\sigma(I)$ ]
<i>R</i>	0.0746	0.0599	0.0556	0.0626	0.0626
<i>R<sub>w</sub></i>	0.1084	0.0700	0.0725	0.0766	0.1162

The structure of  $(^H\text{O})^-$  is in great contrast to that of its *N*-methylated analogue  $(^{\text{Me}}\text{O})^-$ . First, the anion is quasi-planar with phenol/imidazole twist angles of about 1 and 12° for the two molecules in the asymmetric unit. Second, the C1–O1 bond lengths of the two molecules of 1.363(3) and 1.364(3) Å are too long for a phenolate C–O bond, and are characteristic of a protonated phenol (e.g., C1–O1 1.367(3) Å in  $^H\text{OH}$ ). Third, the two C–N bonds of the benzimidazole ring of  $(^H\text{O})^-$  (1.355(3)/1.351(3) Å and 1.361(3)/1.345(3) Å for the two molecules in the asymmetric unit) are significantly different to the corresponding bonds in the phenol parent, which displays a typical imidazole pattern with a short C=N bond (1.326(3) Å in  $^H\text{OH}$  and 1.328(2) and 1.329(2) Å for the two molecules in  $^H\text{OH}\cdot 0.5\text{H}_2\text{O}^{[10]}$ ) and a long C–N bond (1.368(3) Å in  $^H\text{OH}$  and 1.363(2) and 1.358(2) Å for the two molecules in  $^H\text{OH}\cdot 0.5\text{H}_2\text{O}^{[10]}$ ). Therefore, the structural data are consistent with  $(^H\text{O})^-$  being best described as a phenol–imidazolate conjugate anion. The latter establishes OH...N hydrogen-bonding between the phenol OH group and the adjacent imidazolate N atom, as evidenced by the O...N distance of 2.527 Å and the O1–H1...N1 angles of 148.0 and 149.8°. This OH...N<sup>−</sup> tautomeric form is unexpected and unprecedented. Considering the  $pK_a$  of a free phenol/phenolate of about 10 and that of a free imidazole/imidazolate of about 14.5,<sup>[20]</sup> deprotonation would occur at the most acidic site, that is, the phenol site, to produce a phenolate–imidazole conjugate, as assigned recently by Moore et al.<sup>[16]</sup> for  $(^H\text{O})^-$  in solution state. We show here that the presence of a hydrogen bond significantly alters the  $pK_a$  values, making the phenol–imidazolate form isolable. Further reaction of the anion with iodomethane in stoichiometric amount leads to methylation at the N position and not the O position, confirming that the imidazolate form is relevant in solution. The discrepancy between this structure and the previous assignment of  $(^H\text{O})^-$  as a phenolate–benzimidazole compound in solution<sup>[16]</sup> prompted us to investigate the relevance of the two forms by DFT methods (see Supporting Information). We optimised the structures of  $(^H\text{O})^-$  with the proton removed from either the phenol or the benzimidazole group and calculated the energy difference between the two forms. The computed energy gap between the two forms is small (5.0 kJ mol<sup>−1</sup> in the favour of the phenol–imidazolate form), and thus suggests that both forms are relevant and might exist in equilibrium in solution, as further suggested by NMR and electrochemical studies.

Therefore, the oxygen atom is systematically involved in hydrogen-bonding interactions in the series, and only the nature of this bond differs from one compound to another: Intramolecular with OH as the donor in  $^H\text{OH}$ ,  $^{\text{Me}}\text{OH}$  and  $(^H\text{O})^-$ , intermolecular with O<sup>−</sup> as acceptor in  $(^{\text{Me}}\text{O})^- \cdot 2.4\text{H}_2\text{O}$  and intermolecular with OH as donor in  $^{\text{pMe}}\text{OH}$ .

**NMR studies:** The solid-state structures of phenolic compounds  $^H\text{OH}\cdot 0.5\text{H}_2\text{O}$ ,<sup>[10]</sup>  $^H\text{OH}$  and  $^{\text{Me}}\text{OH}$  all involve a intramolecular hydrogen bond between the phenol OH group and benzimidazole N atom. However, polymorphism and

relatively large phenol–imidazole twist angles preclude accurate determination of the strength of this hydrogen-bonding. In solution in CDCl<sub>3</sub>, <sup>1</sup>H NMR spectroscopy is informative. In particular, the OH proton resonances for  $^H\text{OH}$  and  $^{\text{Me}}\text{OH}$  appear at 13.60<sup>[10]</sup> and 12.48 ppm, respectively. Such a high chemical shifts of the phenolic OH protons unambiguously indicate relatively strong hydrogen-bonding in both compounds, and that the latter hydrogen bond is weaker than the former. The hydrogen bond is intramolecular, as evidenced by the fact that the OH resonance remains unaffected even at high dilution. Thus, for all phenol compounds, the intramolecular OH...N hydrogen bond is clearly maintained in solution. In contrast, in the <sup>1</sup>H NMR spectrum of  $(^H\text{O})^-$  no OH resonance was observed. Attempts to discriminate between the imidazolate and phenolate forms of  $(^H\text{O})^-$  in solution by variable-temperature NMR failed, as neither the OH nor the NH proton could be located even at 233 K in CDCl<sub>3</sub>. This certainly indicates fast prototropic exchange between the two forms.

**Electrochemistry:** The electrochemical behaviour of  $^{\text{Me}}\text{OH}$ ,  $^{\text{pMe}}\text{OH}$ ,  $(^{\text{Me}}\text{O})^-$ ,  $(^H\text{O})^-$ <sup>[16]</sup> and  $(^{\text{pMe}}\text{O})^-$  was studied by cyclic voltammetry (CV) in the non-coordinating solvent CH<sub>2</sub>Cl<sub>2</sub> in the presence of 0.1 M tetrabutylammonium perchlorate (TBAP) as supporting electrolyte. All potentials are given relative to the ferrocene/ferrocenium (Fc/Fc<sup>+</sup>) redox couple, which was used as reference (Table 2).

Table 2. Oxidation potentials of the neutral and anionic compounds.<sup>[a]</sup>

Neutral compounds	$E_{1/2}$ [V] ( $\Delta E_p$ ) <sup>[b]</sup>	Anionic compounds <sup>[c]</sup>	$E_{1/2}$ [V] ( $\Delta E_p$ )
$^H\text{OH}$	+0.46 (0.14)	$(^H\text{O})^-$	−0.23 (0.12)
$^{\text{Me}}\text{OH}$	+0.48 (0.18)	$(^{\text{Me}}\text{O})^-$	−0.42 (0.15)
$^{\text{pMe}}\text{OH}$	$E_p^a = +0.33$ $E_p^c = -0.27$ <sup>[d]</sup>	$(^{\text{pMe}}\text{O})^-$	−0.51 (0.14)

[a] At 298 K in CH<sub>2</sub>Cl<sub>2</sub> + 0.1 M TBAP versus Fc/Fc<sup>+</sup>. [b] The  $\Delta E_p$  for the Fc/Fc<sup>+</sup> couple under our experimental conditions is 0.10 V. [c] In the presence of one equivalent of *n*Bu<sub>4</sub>NOH. [d] Irreversible process.

The CV of  $^{\text{Me}}\text{OH}$  is shown in Figure 4a and compared to that of the previously described  $^H\text{OH}$ .<sup>[10]</sup> In both cases the CV consists of a quasi-reversible one-electron oxidation process attributed to a proton-coupled electron-transfer process [PET, see Eq. (1)]<sup>[11,12]</sup> leading to formation of cation  $(^R\text{OH})^{+\bullet}$ , which is stable on the timescale of the experiment (at 298 K). The  $E_{1/2}$  value obtained for  $^{\text{Me}}\text{OH}$  (0.48 V vs. Fc/Fc<sup>+</sup>) is very close to that reported for  $^H\text{OH}$  (0.46 V vs. Fc/Fc<sup>+</sup>, see Table 2). Thus, as for the oxidation of  $^H\text{OH}$ , that of  $^{\text{Me}}\text{OH}$  involves transfer of the phenolic proton to the benzimidazole moiety, and the resulting species is a phenoxyl radical whose oxygen atom is hydrogen-bonded to the benzimidazolium proton. Based on the similarities between  $^H\text{OH}$  and  $^{\text{Me}}\text{OH}$ , from both structural and electrochemical (similar  $E_{1/2}$  values) points of view, it is reasonable to assume that oxidation of  $^{\text{Me}}\text{OH}$  also occurs in a CPET process affording the hydrogen-bonded phenoxyl radical  $(^{\text{Me}}\text{OH})^{+\bullet}$  [see

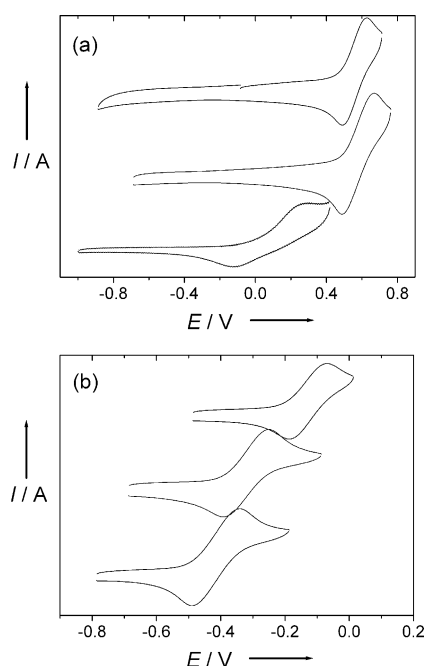
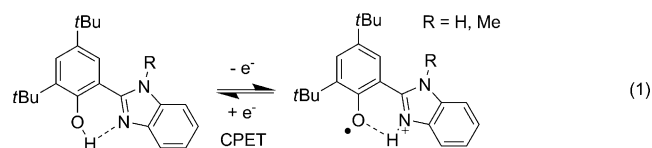


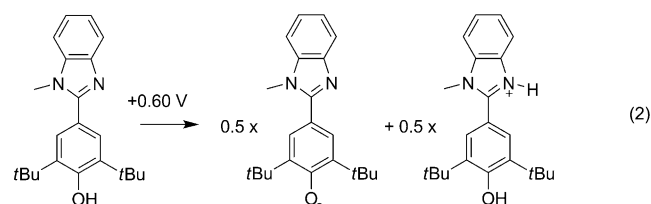
Figure 4. Cyclic voltammetry curves of 0.8–1 mM solutions of  $\text{H}_2\text{O}$  (top),  $\text{MeOH}$  (middle),  $\text{pMeOH}$  (bottom) in  $\text{CH}_2\text{Cl}_2$  (+0.1 M TBAP) in the absence (a) or presence (b) of one molar equivalent of  $[\text{nBu}_4\text{N}][\text{OH}]$  at 298 K ( $iR$ -compensated); scan rate:  $0.1 \text{ V s}^{-1}$ . Potentials are referred to  $\text{Fc}/\text{Fc}^+$ .

Eq. (1)]. This indicates that the presence of the *N*-methyl group at the benzimidazole ring does not significantly affect the formation of the radical. This is consistent with the fact that the intramolecular hydrogen-bonding interaction is preserved in solution for  $\text{MeOH}$ , as evidenced by NMR data, which is crucial for the PET process to proceed in a concerted manner and at relatively low potential. However, the slightly lower  $E_{1/2}$  value for  $\text{H}_2\text{O}$  compared to  $\text{MeOH}$ , may account for the difference in strength of the hydrogen bonds, which is weaker for  $\text{MeOH}$  than for  $\text{H}_2\text{O}$ .

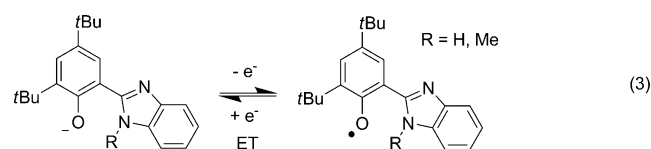


The CV of  $\text{pMeOH}$  contrasts sharply with that of  $\text{MeOH}$  since the oxidation process is not reversible. It displays an anodic peak at  $E_p^a = +0.33 \text{ V}$  versus  $\text{Fc}/\text{Fc}^+$  which is associated with a cathodic peak at the much lower potential value of  $E_p^c = -0.27 \text{ V}$  versus  $\text{Fc}/\text{Fc}^+$ . This evidences either slow electrode kinetics or the existence of a coupled chemical reaction (e.g., a proton transfer to the *N*-methylbenzimidazole base). To gain insight into the redox process, we performed an electrolysis at  $+0.60 \text{ V}$  at 233 K. The experiment was stopped when the intensity of the current was less than 5% of the initial value, which corresponds to removal of 0.5

electrons. The fact that no more than 0.5 electrons could be removed was confirmed by amperometric titration with a rotating disc electrode (RDE; see Supporting Information). Importantly, the colour of the solution at the end of electrolysis was found to be similar (although less intense) to that obtained after electrolysis in the presence of one equivalent of  $\text{nBu}_4\text{NOH}$  (see below). We therefore suggest that the redox process at  $+0.33 \text{ V}$  corresponds to formation of phenoxyl radical species ( $^{\text{pMe}}\text{O}^\bullet$ ) in an intermolecular PET process. Here the *N*-methylbenzimidazole moiety acts as an intermolecular base,<sup>[21]</sup> affording half an equivalent of ( $^{\text{pMe}}\text{O}^\bullet$ ) and half an equivalent of the harder to oxidise *N*-methylbenzimidazolium ( $^{\text{pMe}}\text{OH}_2^+$ ) form of the phenolic compound [Eq. (2)].



Addition of one equivalent of  $\text{nBu}_4\text{NOH}$  to the phenolic compounds results in formation of the anions ( $^{\text{Me}}\text{O}^-$ ), ( $^{\text{pMe}}\text{O}^-$ ) and ( $^{\text{H}}\text{O}^-$ ). In contrast to the PET mechanism characterising oxidation of hydrogen-bonded phenols, oxidation of the phenolate compounds occurs in a simple ET process [Eq. (3)]. A one-electron reversible oxidation process corresponding to the generation of a phenoxyl radical is obtained at  $E_{1/2} = -0.23 \text{ V}$  and  $-0.42 \text{ V}$  versus  $\text{Fc}/\text{Fc}^+$  for ( $^{\text{H}}\text{O}^-$ )<sup>[16]</sup> and ( $^{\text{Me}}\text{O}^-$ ), respectively. Identical results were obtained for the synthetically prepared ( $^{\text{H}}\text{O}^-$ ) and ( $^{\text{Me}}\text{O}^-$ ).



These values are much lower than that obtained for the phenol–benzimidazole parent as a result of the negative charge of the compounds<sup>[20]</sup> and differences in the oxidation mechanism (ET versus CPET). Most importantly, whilst the oxidation potentials of  $\text{H}_2\text{O}$  and  $\text{MeOH}$  were found to be almost the same, this is not the case for the corresponding anions ( $^{\text{H}}\text{O}^-$ ) and ( $^{\text{Me}}\text{O}^-$ ) ( $\Delta E_{1/2} = E_{1/2}(^{\text{H}}\text{O}^-) - E_{1/2}(^{\text{Me}}\text{O}^-) = 0.19 \text{ V}$ ). Since ( $^{\text{Me}}\text{O}^-$ ) cannot establish an intramolecular hydrogen bond as it lacks an NH group [Eq. (3)], but ( $^{\text{H}}\text{O}^-$ ) can, for example, in its  $\text{O}^- \cdots \text{HN}$  tautomeric form, the magnitude of  $\Delta E_{1/2}$  reflects, at least partially, the change in hydrogen-bond strength between the oxidised and reduced forms (see thermodynamic cycle in Figure S1 of the Supporting Information).<sup>[12]</sup> The  $\Delta E_{1/2}$  of  $0.19 \text{ V}$  corresponds to  $17.6 \text{ kJ mol}^{-1}$ . Such a value is within the range of the energy

of a hydrogen bond, and thus suggests that the hydrogen bond of one form is very weak. This observation is consistent with the fact that hydrogen-bonding is expected to be stronger for the phenolate form (reduced form) than for the phenoxyl radical form (oxidised form). Indeed, since hydrogen-bond strength is related to the difference in  $pK_a$  values between donor and acceptor, the hydrogen-bond strength is expected to decrease upon oxidation of the phenolate ( $pK_a(\text{PhOH}/\text{PhO}^-) \approx 10$ ) to the phenoxyl radical ( $pK_a(\text{PhOH}^{\bullet+}/\text{PhO}^{\bullet}) \approx 0$ ). Thus, hydrogen-bonding interaction clearly has an effect on the oxidation potential of these phenolate compounds. However, other factors may contribute to the difference in oxidation potential between  $(^{\text{Me}}\text{O})^-$  and  $(^{\text{H}}\text{O})^-$ , such as 1) the possible contribution of the phenol–benzimidazole tautomer of  $(^{\text{H}}\text{O})^-$  in solution, and 2) the difference in geometry between  $(^{\text{H}}\text{O})^-$  and  $(^{\text{Me}}\text{O})^-$ , particularly in the phenolate/benzimidazole twist angle, which would thereby induce differences in resonance stabilisation. The latter contribution is further evidenced by the  $E_{1/2}$  difference (ca. 0.09 V) between  $(^{\text{Me}}\text{O})^-$  and  $(^{\text{pMe}}\text{O})^-$ , which reflects changes in resonance stabilisation as described in detail below.

**One-electron oxidised species:** The one-electron oxidised species were generated electrochemically in  $\text{CH}_2\text{Cl}_2$  at 243 K and characterised by EPR and UV/Vis spectroscopy. Upon oxidation the colourless solutions of the phenol and phenolate compounds turn green or blue. The UV/Vis spectra (Figure 5) of the electrochemically generated species  $(^{\text{H}}\text{OH})^{\bullet+}$ ,  $(^{\text{Me}}\text{OH})^{\bullet+}$ ,  $(^{\text{H}}\text{O})^{\bullet}$  and  $(^{\text{Me}}\text{O})^{\bullet}$  all display a sharp absorption in the 370–470 nm region, together with a broader and less intense band at longer wavelengths (650–900 nm); see Table 3. These are typical  $\pi$ – $\pi^*$  features of phenoxyl radical compounds<sup>[10,14,17,22]</sup> and confirm the phenoxyl radical character of the oxidised species. Interestingly, the band at about 420 nm observed for the radical cations  $(^{\text{H}}\text{OH})^{\bullet+}$ <sup>[10]</sup> and  $(^{\text{Me}}\text{OH})^{\bullet+}$  [434 (1520) and 416 nm (2350  $\text{M}^{-1}\text{cm}^{-1}$ ), respectively] appears to be red-shifted for the corresponding neutral radicals  $(^{\text{H}}\text{O})^{\bullet}$  and  $(^{\text{Me}}\text{O})^{\bullet}$  [468 (1420) and 467 nm (1270  $\text{M}^{-1}\text{cm}^{-1}$ ), respectively], which indicates an increase in

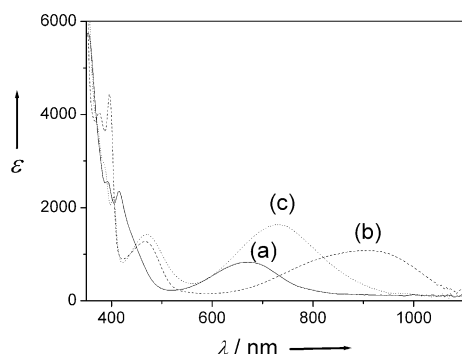


Figure 5. UV/Vis spectra of 0.1–0.18 mM solutions of electrochemically generated  $(^{\text{Me}}\text{OH})^{\bullet+}$  (a, solid),  $(^{\text{H}}\text{O})^{\bullet}$  (b, dashes) and  $(^{\text{Me}}\text{O})^{\bullet}$  (c, dots) at 288 K in  $\text{CH}_2\text{Cl}_2$ .

Table 3. Electronic properties of the radical compounds.<sup>[a]</sup>

Compound	$\lambda_{\text{max}}$ [nm] ( $\epsilon$ [ $\text{M}^{-1}\text{cm}^{-1}$ ])
$(^{\text{H}}\text{OH})^{\bullet+}$	368 (3810), 398 (3780), 434 (1520), 790 (820)
$(^{\text{Me}}\text{OH})^{\bullet+}$	353 (5750), 392sh (2520), 416 (2350), 671 (830)
$(^{\text{H}}\text{O})^{\bullet}$	374 (4040), 395 (4440), 467 (1270), 910 (1080)
$(^{\text{Me}}\text{O})^{\bullet}$	371sh (3840), 386sh (2930), 404 (2245), 468 (1420), 728 (1640)
$(^{\text{pMe}}\text{O})^{\bullet}$	347 (14190), 367 (17390), 384 (28250), 600br (6520)

[a] In  $\text{CH}_2\text{Cl}_2$  + 0.01 M TBAP (UV/Vis).

the energy of the HOMO upon deprotonation of the radical cation and thereby a decrease in the HOMO–LUMO energy gap. Such a red shift is also observed for the longer-wavelength absorption (650–900 nm). Thus the neutral phenoxyl radical is clearly spectroscopically distinguishable from its cationic counterpart.

The spectra obtained after electrochemical oxidation of solutions of  $(^{\text{pMe}}\text{OH})$  and  $(^{\text{pMe}}\text{O})^-$  are shown in Figure 6.

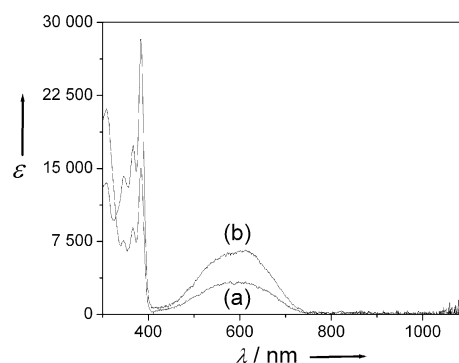


Figure 6. UV/Vis spectra after electrochemical oxidation at 243 K of solutions of  $(^{\text{pMe}}\text{OH})$  (a) and  $(^{\text{pMe}}\text{O})^-$  (b).  $E_{\text{applied}}$  was +0.40 V and –0.20 V, respectively. Electrolysis was stopped when the current was less than 5% of the original value. The spectra were recorded at 243 K ( $l = 1.000$  cm) in 0.07 mM solutions, and the molar extinction coefficients calculated on the basis of the initial concentration of the phenol compound.

Both spectra are remarkably similar in the 330–1100 nm region, which suggests formation of the same chromophore in both cases. Both spectra exhibit a broad band at 600 nm and sharp absorptions at 384 and 367 nm, which correspond to the  $\pi$ – $\pi^*$  transitions of phenoxyl radicals.<sup>[22]</sup> However, all of the transitions are of double the intensity for electrolysed  $(^{\text{pMe}}\text{O})^-$  than for electrolysed  $(^{\text{pMe}}\text{OH})$ . Considering that electrolysis in the presence of base is achieved with a >90% yield (based on RDE voltammetry, see Supporting Information), the spectrum obtained after oxidation of  $(^{\text{pMe}}\text{O})^-$  is attributed to  $(^{\text{pMe}}\text{O})^{\bullet}$ . Since  $(^{\text{pMe}}\text{OH})$  does not absorb significantly (compared to phenoxyl radical species) above 350 nm, the UV/Vis data indicate that only half of the amount of  $(^{\text{pMe}}\text{OH})$  is oxidised to  $(^{\text{pMe}}\text{O})^{\bullet}$  in the absence of exogenous base. The remaining part of the compound is likely in the phenol–benzimidazolium form. This confirms the electrochemical behaviour of  $(^{\text{pMe}}\text{OH})$  presented above [see Eq. (2)], that is, oxidation of  $(^{\text{pMe}}\text{OH})$  is accompanied by intermolecular proton transfer.

The X-band EPR spectra of fluid solutions of electrochemically generated  $(^H\text{OH})^{\bullet+}$ ,<sup>[10]</sup>  $(^{\text{Me}}\text{OH})^{\bullet+}$ ,  $(^H\text{O})^{\bullet}$  and  $(^{\text{Me}}\text{O})^{\bullet}$  are remarkably similar. They consist of an unresolved  $S=1/2$  radical signal centred at  $g=2.005$ , with a line width (peak-to-peak) of about 0.4 mT (see Supporting Information). Though the lack of hyperfine features precludes information on the geometric (such as in phenoxyl–tertiary ammonium systems)<sup>[17]</sup> and electronic structure of the phenoxyl radicals, the relatively small line width most likely indicates that the unpaired electron is not (or to a very little extent) delocalised at the benzimidazole ring. In contrast, the spectrum of  $(^{\text{pMe}}\text{O})^{\bullet}$  displays hyperfine structure due to the interaction of the electron spin with nuclei of the benzimidazole moiety.<sup>[23]</sup> Therefore, the spin density is more delocalised over the benzimidazole rings when this substituent is located in *para* position of the phenoxyl group. The spectrum of  $(^{\text{pMe}}\text{O})^{\bullet}$  (Figure 7) could be simulated using the hyperfine coupling constants  $A_{\text{H}}=6.0$  (for 2 H atoms),  $A_{\text{H}}=2.4$ ,  $A_{\text{H}}=2.9$  and  $A_{\text{N}}=5.5$  MHz. Density functional calculations at the B3LYP level of theory (see below) satisfactorily reproduce this set of values and give further insight into the sign of the hyperfine constants. The computed values are  $A_{\text{H}}=6.0$ ,  $A_{\text{H}}=6.4$ ,  $A_{\text{H}}=-3.0$ ,  $A_{\text{H}}=-4.8$ ,  $A_{\text{N}}=4.6$  and  $A_{\text{N}}=2.9$  MHz. Their assignment is as follows: The hydrogen hyperfine constants higher than 6.0 MHz correspond to the two *meta* hydrogen atoms of the phenoxyl groups, and the others to H atoms located on resonant positions of the benzimidazole ring (Figure 7). Finally, the larger nitrogen hyperfine constant corresponds to the iminic nitrogen atom N1.<sup>[23]</sup>

**Geometric and electronic structures of the radical species by DFT methods:** The geometric structures of the oxidised radical species were investigated by theoretical calculations at the B3LYP level of theory (Figures 8 and 9). The atom numbering used in the text is shown in Table 4. The nature of the SOMO and the corresponding unpaired spin-density distribution were also investigated for all optimised structures. (Figures 10 and 11, Table 4).

**Radical cations  $(^H\text{OH})^{\bullet+}$  and  $(^{\text{Me}}\text{OH})^{\bullet+}$ :** Similarly to previous works on  $(^H\text{OH})^{\bullet+}$ <sup>[10]</sup> we considered two forms for  $(^{\text{Me}}\text{OH})^{\bullet+}$ , in which the proton is either located on the phenoxyl oxygen (i.e.,  $\text{OH}^{\bullet+}\cdots\text{N}$ , form I) or on the *N*-benzimidazole imine nitrogen atom, (i.e.,  $\text{O}^{\bullet+}\cdots\text{HN}$ ,

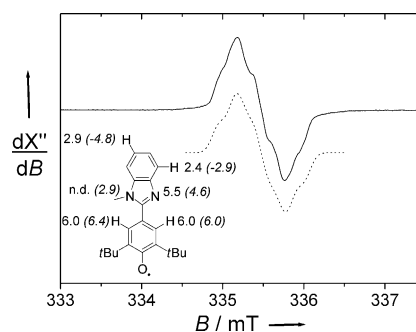


Figure 7. X-band EPR spectrum of  $(^{\text{pMe}}\text{O})^{\bullet}$  at 298 K in  $\text{CH}_2\text{Cl}_2$ :DMSO (1:9). Modulation amplitude 0.05 mT, modulation frequency 100 KHz, microwave frequency 9.42 GHz, power 10 mW. Solid line: experimental spectrum; dotted line: simulation performed by using the hyperfine constants indicated in the inset (in MHz). The values in parentheses are computed values obtained from B3LYP calculations.

form II; Figure 8). The energy calculations (including electronic and solvation terms) reveal that form II is more stable than form I by  $33.1 \text{ kJ mol}^{-1}$ . Therefore,  $(^{\text{Me}}\text{OH})^{\bullet+}$  could be described as a phenoxyl radical hydrogen-bonded to a benzimidazolium group, as for  $(^H\text{OH})^{\bullet+}$ <sup>[10]</sup> and other phenoxyl–tertiary ammonium systems.<sup>[17]</sup> Examination of the geometry optimised form II shows a quinonoid pattern in the phenoxyl ring, that is, the  $\text{C}_{\text{ortho}}\text{--C}_{\text{meta}}$  bonds are short (1.381 and 1.392 Å) with a strong double-bond character,

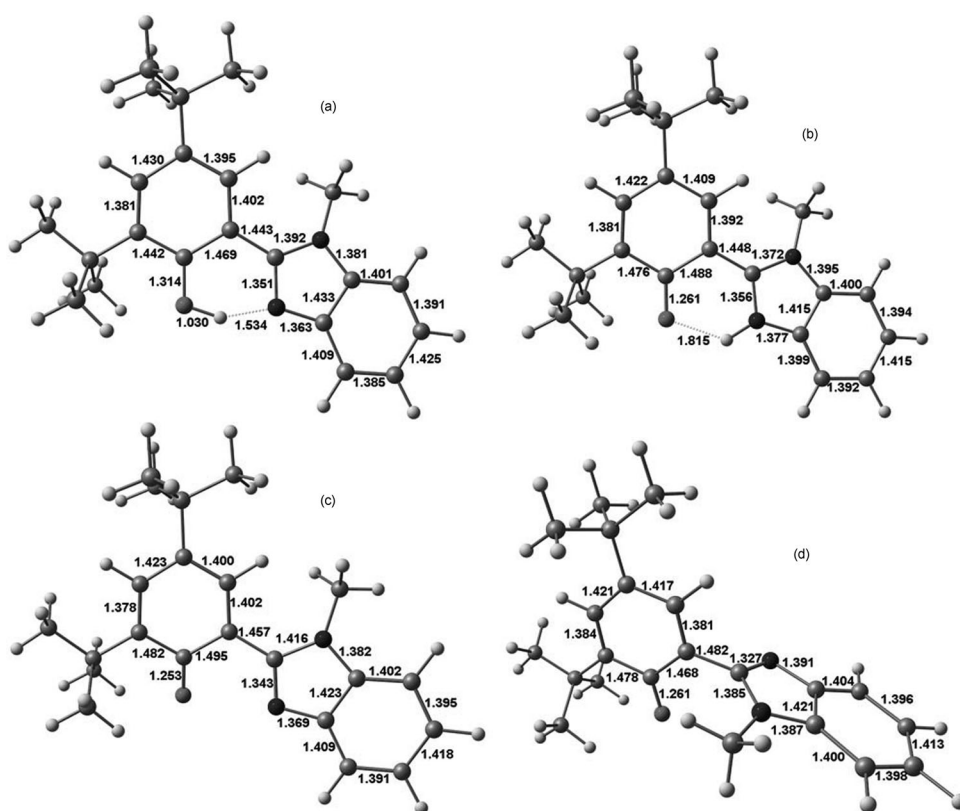


Figure 8. Optimised structures and selected bond lengths [Å] for a)  $(^{\text{Me}}\text{OH})^{\bullet+}$  form I, b)  $(^{\text{Me}}\text{OH})^{\bullet+}$  form II, c)  $(^{\text{Me}}\text{O})^{\bullet}$  form III, d)  $(^{\text{Me}}\text{O})^{\bullet}$  form IV.

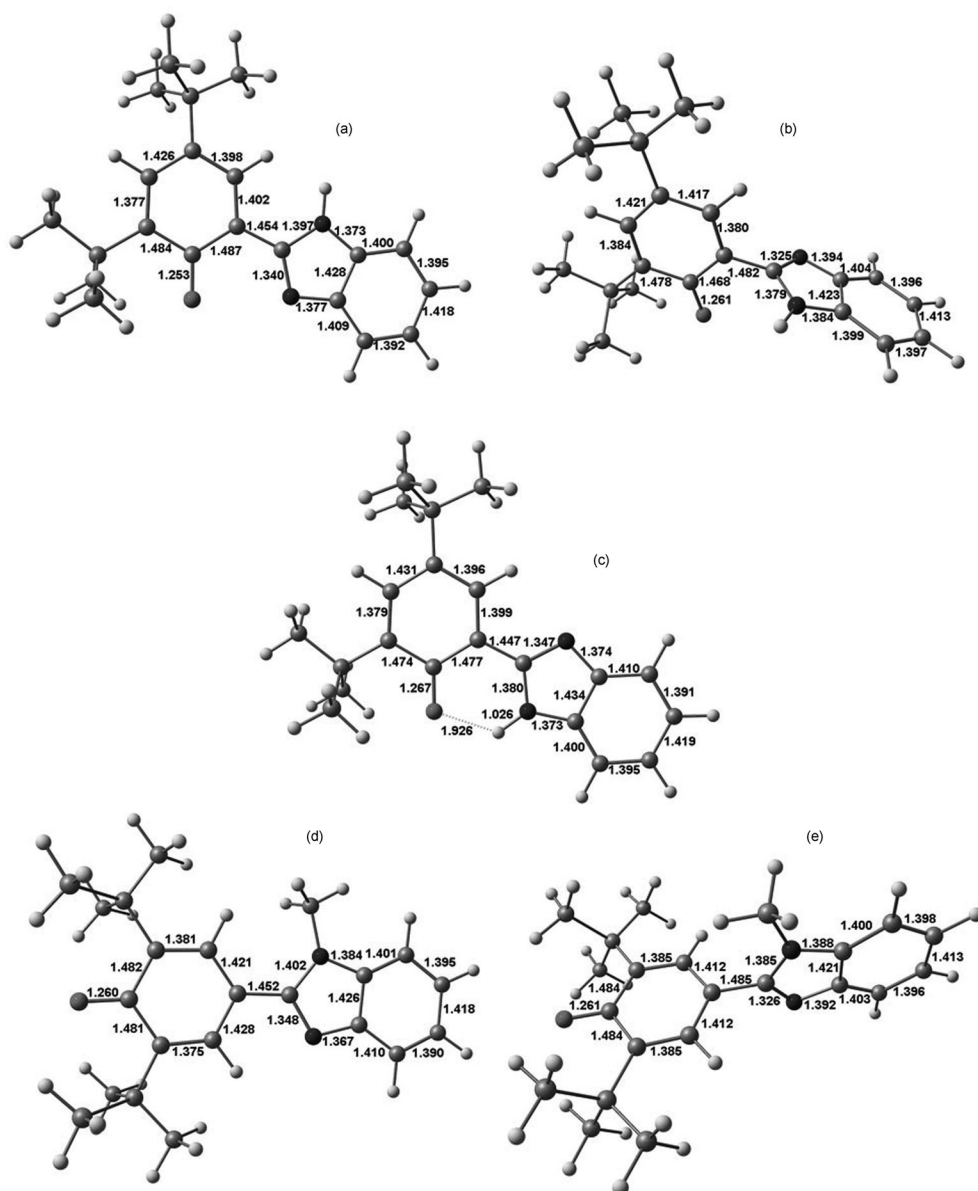


Figure 9. Optimised structures and selected bond lengths [Å] for a) ( $^{p\text{MeO}}\text{O}^\bullet$ ) form V, b) ( $^{p\text{MeO}}\text{O}^\bullet$ ) form VI, c) ( $^{\text{H}\bullet\text{O}}\text{O}^\bullet$ ) form VII, d) ( $^{\text{H}\bullet\text{O}}\text{O}^\bullet$ ) form VIII, e) ( $^{\text{H}\bullet\text{O}}\text{O}^\bullet$ ) form IX, f) ( $^{\text{H}\bullet\text{O}}\text{O}^\bullet$ ) form X.

whereas the other C–C bonds are long (1.409–1.488 Å) with significant single-bond character. The C–O bond length (1.261 Å) is significantly shorter than those of the neutral and zwitterionic forms of  $^{\text{MeO}}\text{OH}$  (1.356 and 1.293 Å, respectively; see Supporting Information). These results are in agreement with the few available X-ray structures for phenoxyl radicals.<sup>[25]</sup> The phenoxyl radical character of form II of ( $^{\text{MeO}}\text{OH})^{+\bullet}$ , as for form II ( $^{\text{H}\bullet\text{O}}\text{OH})^{+\bullet}$ ,<sup>[10]</sup> is further confirmed by the SOMO, which is mainly located on the phenoxyl ring. Consequently most of the positive spin density resides on the phenoxyl ring, and is distributed at the O,  $\text{C}_{\text{ortho}}$  and  $\text{C}_{\text{para}}$  atoms (i.e., O 0.28, C2 and C4 0.18, C6 0.21), as expected for phenoxyl radical species (Figure 10 and Table 4). The relatively high spin density at the *ipso* carbon atom (C1

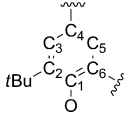
0.08) is characteristic of hydrogen-bonded phenoxyl radicals.<sup>[26]</sup>

In contrast, in the least stable form I, significant delocalised of the SOMO on the *N*-methylbenzimidazole ring indicates a non-negligible benzimidazolyl radical character.

*The ortho- and para- substituted neutral radicals ( $^{\text{MeO}}\text{O}^\bullet$  and ( $^{p\text{MeO}}\text{O}^\bullet$ ):* For the neutral radical ( $^{\text{MeO}}\text{O}^\bullet$ ), we considered two forms, namely, III and IV, which differ in the orientation of the benzimidazole ring (Figure 8). In form III the phenoxyl and benzimidazole rings are coplanar and the N–CH<sub>3</sub> and C–O bonds are *trans* to one another, whereas in form IV the phenoxyl and benzimidazole rings are orthogonal to one another. Form IV is more stable by 32.0 kJ mol<sup>−1</sup>. This is consistent with the structurally characterised parent anion ( $^{\text{MeO}}\text{O}^-$ ) showing a significant phenol/benzimidazole twist (see Figure 3d). Thus, as for ( $^{\text{MeO}}\text{O}^-$ ), the large energy difference between the two radical forms of ( $^{\text{MeO}}\text{O}^\bullet$ ) (twisted and planar) likely arises from steric hindrance between the methyl group and the adjacent phenoxyl *meta* hydrogen atom. It is instructive to compare the distribution of bond lengths within the phenoxyl ring in forms III and IV. In the twisted form IV, a quinonoid distribution of

bond lengths is observed with almost identical and short C2–C3 and C5–C6 bond lengths (1.384 and 1.381 Å, respectively) and long C1–C2, C3–C4, C4–C5 and C1–C6 bond lengths (1.478, 1.421, 1.417 and 1.468 Å respectively). In the planar form III, the same overall pattern is observed, although it is less symmetrical. For instance, the C2–C3 and C5–C6 bond lengths differ by 0.025 Å (1.378 and 1.403 Å respectively), and the C3–C4 and C4–C5 bond lengths by 0.023 Å (1.423 and 1.400 Å respectively). The C–O bond length in form III is shorter than that in IV (1.253 and 1.261 Å respectively). This dissymetrisation in the C–C bond lengths is a consequence of planarity and subsequent resonance effects in form III. Indeed, the SOMO of form III is significantly delocalised on the benzimidazole ring (87%

Table 4. Spin populations on selected atoms and numbering.



Compound	O	C1	C2	C4	C6
( <sup>Me</sup> OH) <sup>++</sup> , form I	0.15	0.18	0.02	0.18	0.15
( <sup>Me</sup> OH) <sup>++</sup> , form II	0.28	0.08	0.18	0.21	0.18
( <sup>Me</sup> O) <sup>+</sup> , form III	0.30	0.06	0.15	0.20	0.15
( <sup>Me</sup> O) <sup>+</sup> , form V	0.32	0.08	0.18	0.22	0.18
( <sup>Me</sup> O) <sup>+</sup> , form IV·H <sub>2</sub> O	0.31	0.06	0.16	0.21	0.16
( <sup>pMe</sup> O) <sup>+</sup> , form V	0.30	0.06	0.13	0.20	0.17
( <sup>pMe</sup> O) <sup>+</sup> , form VI	0.32	0.08	0.18	0.22	0.18
( <sup>H</sup> O) <sup>+</sup> , form VII	0.30	0.06	0.16	0.20	0.16
( <sup>H</sup> O) <sup>+</sup> , form VIII	0.32	0.08	0.18	0.23	0.18
( <sup>H</sup> O) <sup>+</sup> , form IX	0.30	0.06	0.13	0.20	0.17
( <sup>H</sup> O) <sup>+</sup> , form X	0.10	0.12	<0.02	0.06	0.09

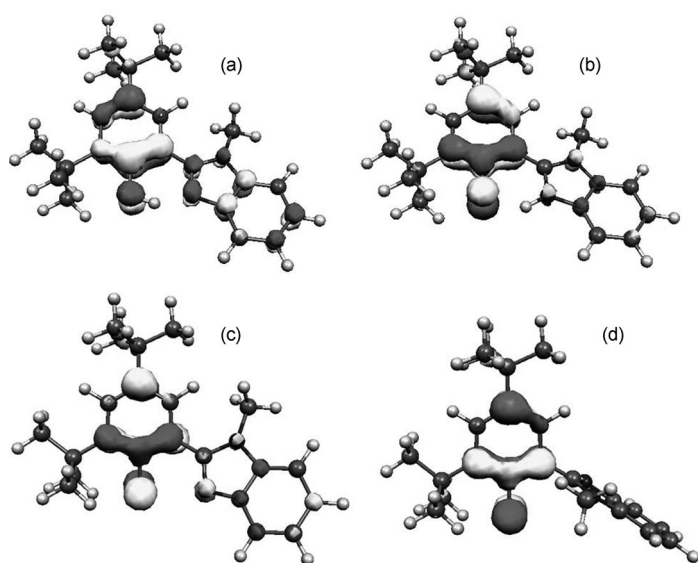


Figure 10. Composition of the SOMO of a) (<sup>Me</sup>OH)<sup>++</sup> form I, b) (<sup>Me</sup>OH)<sup>++</sup> form II, c) (<sup>Me</sup>O)<sup>+</sup> form III, d) (<sup>Me</sup>O)<sup>+</sup> form IV.

phenoxy and 13 % benzimidazole contributions), whereas that of form IV is mainly (99 %) located on the phenoxy ring (see Figure 10). Nevertheless, both forms preserve a phenoxy radical quinoid pattern with positive spin populations mainly distributed on the O, C1, C2, C4 and C6 atoms, but the individual atom contributions are slightly lower for form III than for form IV (0.30/0.32, 0.06/0.08, 0.15/0.18, 0.20/0.22, 0.15/0.18 respectively; see Table 4). Also, a non-negligible contribution (0.06) of the iminic nitrogen atom of the *N*-methylbenzimidazole moiety could be evidenced in the planar structure (form III).

The optimised structures of (<sup>pMe</sup>O)<sup>+</sup> in which the *N*-methylbenzimidazole moiety is coplanar with (form V) and orthogonal to (form VI) the phenoxy ring are shown in Figure 9. In contrast to (<sup>Me</sup>O)<sup>+</sup> the lowest-energy form is planar form V (more stable by 9.2 kJ mol<sup>-1</sup>), which evidences stronger stabilisation by resonance effect. A quinonoid

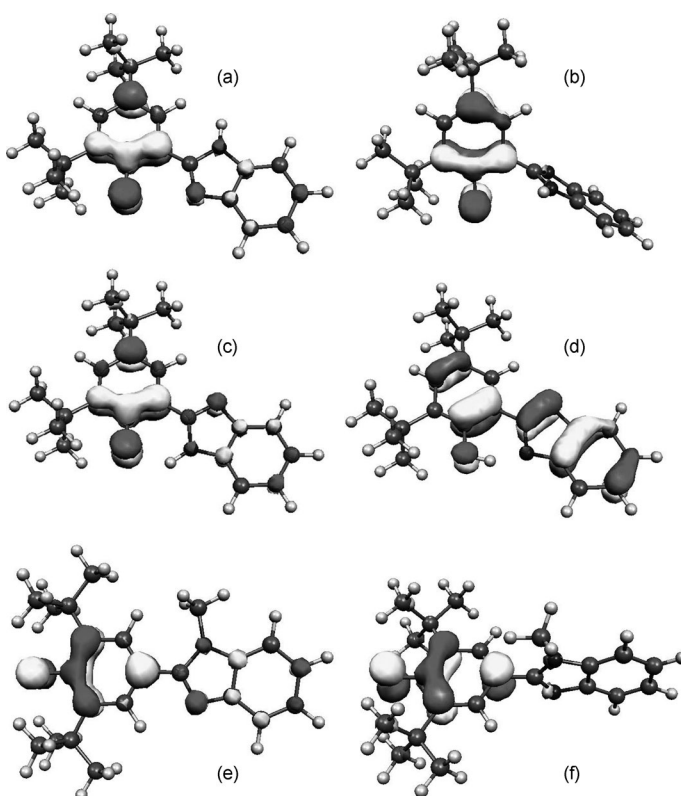


Figure 11. Composition of the SOMO of a) (<sup>pMe</sup>O)<sup>+</sup> form V, b) (<sup>pMe</sup>O)<sup>+</sup> form VI, c) (<sup>H</sup>O)<sup>+</sup> form VII, d) (<sup>H</sup>O)<sup>+</sup> form VIII, e) (<sup>H</sup>O)<sup>+</sup> form IX, f) (<sup>H</sup>O)<sup>+</sup> form X.

distribution of bond lengths is observed within the phenoxy ring in both cases. A remarkable symmetrical pattern is observed along the C1–C4 axis, with the bond lengths in each pair C1–C2/C1–C6, C2–C3/C5–C6 and C3–C4/C4–C5 being quasi-equal for form V and equal for form VI (see Figure 9). Interestingly, the C–O bond length is barely affected by the orientation of the *N*-methylbenzimidazole ring (1.260 Å in form V versus 1.261 Å in form VI). This contrasts with (<sup>Me</sup>O)<sup>+</sup>, in which a significant difference was observed between planar and orthogonal forms (1.253 and 1.261 Å, respectively). The composition of the SOMO of (<sup>pMe</sup>O)<sup>+</sup> in its most stable planar form V is 82 % phenoxy and 18 % *N*-methylbenzimidazole, whereas it is almost exclusively phenoxy (99 %) in the orthogonal form VI (Figure 11). The SOMO of the planar form of (<sup>pMe</sup>O)<sup>+</sup> is more delocalised than that of the planar form of (<sup>Me</sup>O)<sup>+</sup> (87 % phenoxy and 13 % benzimidazole), that is, the contribution of the conjugated *N*-methylbenzimidazole moiety is enhanced when it is located at the *para* rather than at the *ortho* position (Figure 11). Consequently, lower spin populations are found at the phenoxy O, C1, C2, C4 and C6 atoms in form V (0.27, 0.06, 0.13, 0.24, 0.13, respectively, with a 0.06 contribution of the iminic nitrogen atom of the *N*-methylbenzimidazole moiety) than in form VI (0.32, 0.08, 0.18, 0.22, 0.18 respectively, without significant influence of the atoms of the *N*-methylbenzimidazole moiety; see Table 4). The increasing delocalisation of the SOMO in (<sup>pMe</sup>O)<sup>+</sup> compared to (<sup>Me</sup>O)<sup>+</sup>

correlates well with the experimental facts that  $(^{\text{pMe}}\text{O})^\bullet$  is formed at a lower potential than  $(^{\text{Me}}\text{O})^\bullet$  and that the EPR spectrum of  $(^{\text{pMe}}\text{O})^\bullet$  is more expanded than that of  $(^{\text{Me}}\text{O})^\bullet$ .

**Neutral radical  $(^{\text{H}}\text{O})^\bullet$ :** For the radical  $(^{\text{H}}\text{O})^\bullet$  we considered four forms VII–X (Figure 9). Forms VII and VIII are analogous to forms III and IV of  $(^{\text{Me}}\text{O})^\bullet$ ; that is, the phenoxyl and benzimidazole rings are either coplanar with the N–H and C–O bonds being *trans* (form VII), or orthogonal (form VIII) to one another. In form IX the phenoxyl and benzimidazole rings are coplanar with the N–H and C–O bonds being *cis* to one another, thus allowing the formation of an O $\cdots$ HN hydrogen bond. Form X represents the extreme situation in which the proton is located at the phenol group (i.e., OH $^+\cdots$ N $^-$ ), as if it derived directly from one-electron removal from the parent anion  $(^{\text{H}}\text{O})^-$  in its crystallographically characterised OH $\cdots$ N form. The optimised forms VII, VIII and X were found to be of much higher energy (by 31.0, 34.7 and 41.7 kJ mol $^{-1}$ , respectively) than optimised form IX. The stabilisation of form IX may be explained by the interplay of several factors, including the lack of steric hindrance with the phenoxyl *meta* hydrogen atom, the existence of resonance stabilisation and the formation of a hydrogen bond between the phenoxyl oxygen and the N–H group. As expected, the variation of C–C bond lengths and the computed C–O bond lengths in  $(^{\text{H}}\text{O})^\bullet$  in forms VII and VIII are quite similar to that obtained for forms III and IV of  $(^{\text{Me}}\text{O})^\bullet$  and thus will not be commented further. The quinonoid structure of planar hydrogen-bonded form IX resembles that of planar form VII, with similar C2–C3, C3–C4, C4–C5 and C5–C6 bond lengths. However, noticeable differences arising from hydrogen-bonding could be evidenced by careful examination of the C1–C2, C1–C6 and C–O bond lengths: The first two bonds are shortened by 0.01 Å, whereas the last-named is significantly lengthened (+0.015 Å) in form IX. Interestingly, the O $\cdots$ H–N distance of 1.926 Å is significantly larger than those obtained for compounds in which the hydrogen bond is established between a phenoxyl oxygen atom and a cationic benzimidazolium (or *N*-methylbenzimidazolium) group, like  $(^{\text{H}}\text{OH})^{+\bullet}$  and  $(^{\text{Me}}\text{OH})^{+\bullet}$  (1.815 Å), that is, the hydrogen-bonding interaction is stronger when the donor is a cationic partner.

The composition of the SOMO of  $(^{\text{H}}\text{O})^\bullet$  is affected by the relative orientation of the phenoxyl ring with respect to the benzimidazole ring in a similar way to  $(^{\text{Me}}\text{O})^\bullet$ : For an orthogonal orientation of the rings (form VIII) the contributions of the phenoxyl and benzimidazole moieties are 99 and 1% respectively, that is, similar to  $(^{\text{Me}}\text{O})^\bullet$ . When the phenoxyl and benzimidazole rings are coplanar a significant contribution of the benzimidazole ring to the SOMO could be evidenced: The SOMO has 88% phenoxyl and 12% benzimidazole composition when the N–H and C–O bonds are *trans* to one another (form VII), and 85% phenoxyl and 15% benzimidazole ring when the N–H and C–O bonds are *cis* and hydrogen-bonded to one another (form IX). Therefore, the intramolecular hydrogen bond in form IX appears to increase delocalisation of the SOMO over the benzimida-

zole ring. It is noteworthy that the spin populations in forms VII and VIII are very close to those obtained for the corresponding forms III and IV of  $(^{\text{Me}}\text{O})^\bullet$  (Table 4), and this suggests a negligible effect of the methyl substituent on the benzimidazole properties. For the most stable planar hydrogen-bonded form IX, we observed minor changes compared to planar form VII, the main difference being the slightly lower spin population at the C2 atom.

Form X is the highest in energy and represents an extreme case in which a very acidic phenoxyl radical cation is at hydrogen-bonding distance from a basic imidazolate group. This is not a chemically realistic situation, and one would expect a spontaneous intramolecular proton transfer to give form IX. Thus, form X could be regarded as “transition state” upon oxidation of  $(^{\text{H}}\text{O})^-$  (in OH $\cdots$ N form) to  $(^{\text{H}}\text{O})^\bullet$  in form IX (as O $\cdots$ HN). The existence of form X may result from stabilisation of this “transition state” by significant delocalisation of the unpaired electron. This indicates that electronics play a crucial role in the location of the proton in the compound. This also poses the question of the possibility of an unprecedented PET mechanism for oxidation of a phenol–benzimidazole pair in the deprotonated form (see below). The structure of form X differs notably from the other forms of  $(^{\text{H}}\text{O})^\bullet$ . The C–O bond is much longer (1.335 Å), and the phenoxyl C–C bonds do not show a quinonoid pattern (see Figure 9f). Therefore  $(^{\text{H}}\text{O})^\bullet$  in form X exhibits a much smaller phenoxyl radical character. This is further confirmed by the SOMO analysis, which shows a quasi-equal contributions of the phenoxyl (48%) and benzimidazolyl (52%) rings. Accordingly, the spin populations on the O, C1, C2, C4 and C6 atoms (0.10, 0.12, <0.02, 0.06 and 0.09, respectively) are much smaller than those of the other forms (Figure 11f and Table 4).

**High-field EPR:** In the absence of hyperfine couplings, X-band EPR spectroscopy is inefficient in probing the spin distribution of the phenoxyl radical and the electrostatic environment around the phenoxyl O atom. It is known that the anisotropy of the *g* tensor in organic radicals is too small to be detected at 9.4 GHz, but it can be resolved at higher frequencies.<sup>[3]</sup> Thus, we performed EPR measurements at 285 GHz for frozen CH<sub>2</sub>Cl<sub>2</sub> solutions of  $(^{\text{Me}}\text{OH})^{+\bullet}$ ,  $(^{\text{H}}\text{O})^\bullet$  and  $(^{\text{Me}}\text{O})^\bullet$  at 10 K (Table 5). The EPR spectra are shown in Figure 12. For all radical compounds, a rhombic ( $S=1/2$ ) signal is observed, from which the three principal *g* values *g*<sub>1</sub>, *g*<sub>2</sub> and *g*<sub>3</sub> (see Figure 12 inset) are resolved and can be extracted by simulation (see Table 5). Regardless of the compounds investigated, the obtained *g*<sub>2</sub> and *g*<sub>3</sub> values of about 2.0044 and 2.0023, respectively, are invariable, and are identical to those reported for  $(^{\text{H}}\text{OH})^{+\bullet}$ ,<sup>[10]</sup> the tri-*tert*-butylphenoxyl radical<sup>[15]</sup> and phenoxyl radical hydrogen-bonded to a neighbouring ammonium group.<sup>[17]</sup> In contrast, the *g*<sub>1</sub> value varies significantly (Table 5). This behaviour is consistent with the *g*<sub>1</sub> tensor (oriented along the C–O axis, Figure 12) being sensitive to the local environment around the oxygen atom, that is, any changes in the spin density at the oxygen atom, as well as in the energy gap between the

Table 5. Experimental<sup>[a]</sup> and calculated<sup>[b]</sup>  $g$  tensors of the radical compounds.

Compound	$g_1$	$g_2$	$g_3$
( <sup>H</sup> OH) <sup>•+</sup> , exptl	2.0067	2.0043	2.0022
( <sup>Me</sup> OH) <sup>•+</sup> , exptl	2.0069	2.0044	2.0023
( <sup>Me</sup> OH) <sup>•+</sup> , form I calcd	2.0041	2.0038	2.0000
( <sup>Me</sup> OH) <sup>•+</sup> , form II calcd	2.0065	2.0043	2.0023
( <sup>Me</sup> O) <sup>•</sup> , exptl	2.0079	2.0044	2.0023
( <sup>Me</sup> O) <sup>•</sup> , form III calcd	2.0083	2.0043	2.0026
( <sup>Me</sup> O) <sup>•</sup> , form IV calcd	2.0079	2.0045	2.0023
( <sup>Me</sup> O) <sup>•</sup> , form IV·H <sub>2</sub> O calcd <sup>[c]</sup>	2.0071	2.0044	2.0023
( <sup>pMe</sup> O) <sup>•</sup> , exptl	2.0073	2.0043	2.0023
( <sup>pMe</sup> O) <sup>•</sup> , form V calcd	2.0071	2.0046	2.0024
( <sup>pMe</sup> O) <sup>•</sup> , form VI calcd	2.0080	2.0046	2.0024
( <sup>H</sup> O) <sup>•</sup> , exptl	2.0072	2.0044	2.0023
( <sup>H</sup> O) <sup>•</sup> , form VII calcd	2.0084	2.0044	2.0023
( <sup>H</sup> O) <sup>•</sup> , form VIII calcd	2.0080	2.0045	2.0023
( <sup>H</sup> O) <sup>•</sup> , form IX calcd	2.0069	2.0045	2.0022
( <sup>H</sup> O) <sup>•</sup> , form X calcd	2.0037	2.0026	2.0023

[a] In CH<sub>2</sub>Cl<sub>2</sub> + 0.1 M TBAP;  $T = 10$  K. The confidence level on the experimental  $g$  values is 0.0001. [b] EPR parameters were obtained from additional single-point calculations with the hybrid functional B3LYP and the EPR-II basis set (see Experimental Section). [c] At the hydrogen-bond distance of 1.67 Å deduced from the X-ray crystal structure of [<sup>Me</sup>O]<sup>•</sup>·[nBu<sub>4</sub>N]<sup>+</sup>·2.4H<sub>2</sub>O.

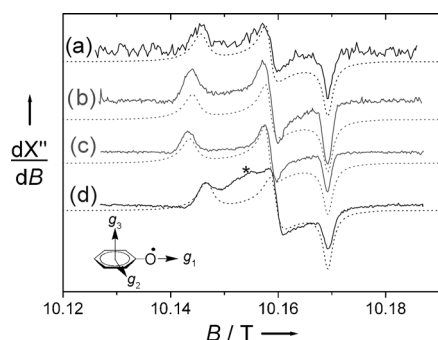


Figure 12. High-field (285 GHz) EPR spectra of electrochemically generated a) (<sup>Me</sup>OH)<sup>•+</sup>, b) (<sup>H</sup>O)<sup>•</sup>, c) (<sup>Me</sup>O)<sup>•</sup> and d) (<sup>pMe</sup>O)<sup>•</sup> recorded as 5 mm CH<sub>2</sub>Cl<sub>2</sub> solutions at 5 K. The star denotes an unidentified paramagnetic impurity.

oxygen  $p_z$  (contributing to the SOMO) and  $p_y$  (lone pair) orbitals will affect the  $g_1$  value.<sup>[3,10]</sup> In the present case, formation of an in-plane hydrogen bond stabilises the  $p_y$  lone pair of the oxygen atom, thereby increasing the energy gap between this orbital and the SOMO. The net result is a decrease in the spin–orbit coupling due to hydrogen-bonding and thus a lowering of the  $g_1$  value.

Thus, in this series of compounds, only the  $g_1$  value is informative for probing local environmental changes on the phenoxyl radical. Consistently, the experimentally determined  $g_1$  value varies as such:  $2.0079 > 2.0073 > 2.0072 > 2.0069 > 2.0067$ <sup>[10]</sup> for (<sup>Me</sup>O)<sup>•</sup>, (<sup>pMe</sup>O)<sup>•</sup>, (<sup>H</sup>O)<sup>•</sup>, (<sup>Me</sup>OH)<sup>•+</sup> and (<sup>H</sup>OH)<sup>•+</sup> respectively (see Table 5). The lowest  $g_1$  values, 2.0067<sup>[10]</sup> and 2.0069, are obtained for (<sup>H</sup>OH)<sup>•+</sup> and (<sup>Me</sup>OH)<sup>•+</sup>, respectively. This evidences a hydrogen bond with a cationic partner which provides a very electropositive environment around the phenoxyl oxygen atom. These values

are within the range of those reported for crystals of strongly hydrogen-bonded  $\gamma$ -irradiated tyrosine·HCl (2.0067),<sup>[27]</sup> the transient TyrD<sup>•</sup> radical (2.0066, Figure 1)<sup>[2]</sup> and other phenoxyl radicals hydrogen-bonded to iminium nitrogen atoms.<sup>[9]</sup> Importantly, they are higher than those reported for strongly intramolecularly hydrogen-bonded phenoxyl–tertiary ammonium systems in which the positive charge is mainly located on the nitrogen atom (2.0061–2.0066).<sup>[17]</sup> Delocalisation of the positive charge over the benzimidazolium ring thus lowers the charge density on the nitrogen atom and makes the oxygen environment less electropositive in (<sup>H</sup>OH)<sup>•+</sup> and (<sup>Me</sup>OH)<sup>•+</sup> than in phenoxyl–tertiary ammonium systems. The calculated  $g_1$  values of (<sup>Me</sup>OH)<sup>•+</sup> for forms I (proton on the phenoxyl oxygen atom) and II (proton on the *N*-methylbenzimidazole moiety) are quite different ( $g_1 = 2.0041$  and 2.0065 respectively; Table 5). Clearly, only the latter set of values reproduces satisfactory the experimental data, and further supports the assumption that (<sup>Me</sup>OH)<sup>•+</sup> is a phenoxyl radical hydrogen-bonded to a cationic partner.

The highest  $g_1$  value (2.0079) is obtained for (<sup>Me</sup>O)<sup>•</sup>, that is, the compound for which the phenoxyl oxygen atom cannot establish any intramolecular hydrogen bond. The computed  $g_1$  value for (<sup>Me</sup>O)<sup>•</sup> in forms III and IV (in which the *N*-methylbenzimidazole and phenoxyl rings are coplanar and orthogonal, respectively) are 2.0083 and 2.0079, respectively (Table 5). The inclusion of a water molecule hydrogen-bonded to the phenoxyl oxygen atom (form IV·H<sub>2</sub>O) results in a dramatic decrease of the  $g_1$ -tensor component (2.0071) which does not account for experimental data. Although the difference in anisotropy is small between forms III and IV, the experimental data are in better agreement with form IV. This indicates that the phenoxyl and *N*-methylbenzimidazole rings are orthogonal in (<sup>Me</sup>O)<sup>•</sup>, in agreement with the energy calculations, and the fact that the oxygen atom establishes no or a very weak hydrogen bond with a water molecule.

The  $g_1$  value of 2.0072 measured for (<sup>H</sup>O)<sup>•</sup> is intermediate between those of (<sup>Me</sup>O)<sup>•</sup> and (<sup>Me</sup>OH)<sup>•+</sup>. The electrostatic environment around the oxygen atom in (<sup>H</sup>O)<sup>•</sup> is therefore less electropositive than in (<sup>Me</sup>OH)<sup>•+</sup> (or (<sup>H</sup>OH)<sup>•+</sup>) but more electropositive than in (<sup>Me</sup>O)<sup>•</sup>. This fact is consistent with the presence of an intramolecular hydrogen bond between the phenoxyl radical oxygen and a neutral partner (benzimidazole group) in (<sup>H</sup>O)<sup>•</sup>. This simple analysis was confirmed by theoretical calculations: The computed  $g_1$  values for (<sup>H</sup>O)<sup>•</sup> in forms VII, VIII and IX (in which the *N*-methylbenzimidazole and phenoxyl rings are coplanar without a hydrogen bond and orthogonal or coplanar with a hydrogen bond, respectively) are 2.0084, 2.0080 and 2.0069, respectively (Table 5). Clearly, hydrogen-bonding interactions between the phenoxyl oxygen atom and the *N*-methylbenzimidazole NH group in form IX decrease significantly the  $g_1$  component. The experimental  $g_1$  value is far from the calculated value for forms VII and VIII but matches well with that of form IX. These results are thus consistent with (<sup>H</sup>O)<sup>•</sup> being a neutral phenoxyl radical species intramolecularly hydrogen-bonded to the benzimidazole NH moiety. Calculations

on form X, in which the proton is located on the phenol group in place of the *N*-benzimidazole moiety, give a  $g_1$  value of 2.0037, which clearly excludes it as experimentally relevant.

The  $g_1$  value obtained for  $(^{\text{pMe}}\text{O})^\bullet$  of 2.0073, is lower than that of  $(^{\text{Me}}\text{O})^\bullet$  (2.0079) (Table 5). The lower  $g_1$  value in  $(^{\text{pMe}}\text{O})^\bullet$  is consistent with  $(^{\text{pMe}}\text{O})^\bullet$  being more delocalised than  $(^{\text{Me}}\text{O})^\bullet$ , since a decrease of the spin density at the O atom decreases this  $g$  component. The calculated  $g_1$  values of 2.0071 and 2.0080 for the planar form V and the orthogonal form VI of  $(^{\text{pMe}}\text{O})^\bullet$ , respectively, confirm this fact. Thus, both the experimental and calculated results suggest that the *para*-substituted radical  $(^{\text{pMe}}\text{O})^\bullet$  is planar, whereas the *ortho*-substituted radical  $(^{\text{Me}}\text{O})^\bullet$  is orthogonal.

Combined HF-EPR data and DFT calculations have thus provided strong evidence that  $(^{\text{Me}}\text{OH})^{+\bullet}$  and  $(^{\text{H}}\text{O})^\bullet$  are phenoxyl radical species in which the oxygen atom establishes an intramolecular hydrogen bond with either a cationic partner or a neutral partner, whereas no such interaction exists in  $(^{\text{Me}}\text{O})^\bullet$  and  $(^{\text{pMe}}\text{O})^\bullet$ .

## Conclusion

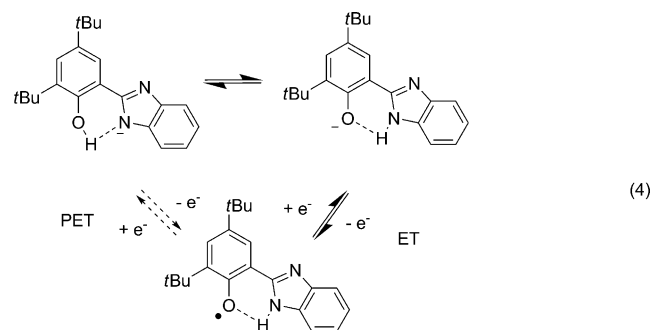
We have shown that  $^{\text{Me}}\text{OH}$  contains a phenolic proton which is intramolecularly hydrogen-bonded to a *N*-methylbenzimidazole group both in solution and at the solid state, similarly to  $^{\text{H}}\text{OH}$ . Its one-electron oxidation occurs by an intramolecular CPET mechanism similar to that proposed for the generation of  $\text{Tyr}_\text{D}^\bullet$  in PSII and affords the phenoxyl *N*-methylbenzimidazolium radical species  $(^{\text{Me}}\text{OH})^{+\bullet}$ . HF-EPR spectroscopy, which allows for resolution of the  $g$ -tensor anisotropy, reveals a small  $g_1$  value (2.0069) consistent with the existence of an intramolecular hydrogen bond between the phenoxyl oxygen atom and the protonated iminic nitrogen atom of the *N*-methylbenzimidazole moiety, as confirmed by complementary DFT calculations.

$^{\text{pMe}}\text{OH}$ , which differs from  $^{\text{Me}}\text{OH}$  in the position of the *N*-methylbenzimidazole substituent (*para* instead of *ortho*), lacks the possibility to establish an intramolecular hydrogen bond between the phenolic proton and the benzimidazole group. Its oxidation occurs in an unprecedented PET mechanism leading to an equimolar mixture of the *N*-methylbenzimidazole-phenoxyl radical  $(^{\text{pMe}}\text{O})^\bullet$  and *N*-methylbenzimidazolium-phenol  $(^{\text{pMe}}\text{OH}_2)^+$  conjugates. Thus, during oxidation, intermolecular proton transfer occurs to the *N*-methylbenzimidazole base, leaving half of the phenol compound (in its acidic  $(^{\text{pMe}}\text{OH}_2)^+$  form) unoxidised. These results show the importance of the spatial separation between the pro-phenoxyl oxygen atom and the acceptor nitrogen atom in determining the mechanism of the oxidation process, as well as the nature of the oxidation products formed. This illustrates the need for a short distance between  $\text{Tyr}_\text{D}$  and the His to improve radical formation in biological systems (Figure 1).

Addition of one equivalent of  $n\text{Bu}_4\text{NOH}$  to  $^{\text{Me}}\text{OH}$  affords  $(^{\text{Me}}\text{O})^-$ , which has been identified as a phenolate-*N*-methyl-

benzimidazole species by X-ray diffraction. Its oxidation potential is much lower than that of the phenol parent as a result of increased electron density at the oxygen atom (negative charge) and differences in the oxidation mechanism (simple ET in this case). Electrochemically generated  $(^{\text{Me}}\text{O})^\bullet$  exhibits a high  $g_1$  value, in accordance with the absence of hydrogen-bonding and a preferred twisted structure which prevents delocalisation of the radical onto the *N*-methylbenzimidazole ring. In contrast, the analogous *para*-substituted radical  $(^{\text{pMe}}\text{O})^\bullet$  appears to be planar and more conjugated than  $(^{\text{Me}}\text{O})^\bullet$ , as evidenced by the experimental electrochemical and EPR data as well as DFT calculations.

In contrast to  $(^{\text{Me}}\text{O})^-$ , X-ray diffraction analysis reveals that  $(^{\text{H}}\text{O})^-$  in the solid state consists of an unprecedented phenol-benzimidazolate and not a phenolate-benzimidazole compound. The energy gap between these two tautomeric forms is small ( $5.0 \text{ kJ mol}^{-1}$ ) and suggests that they are most likely in equilibrium in solution. Remarkably, the one-electron oxidised  $(^{\text{H}}\text{O})^\bullet$  could be unambiguously identified as a phenoxyl-benzimidazole radical species. Its  $g_1$  value is intermediate between those obtained for  $(^{\text{Me}}\text{OH})^{+\bullet}$  and  $(^{\text{Me}}\text{O})^\bullet$ , and thus evidences an intermediate electrostatic environment around the phenoxyl oxygen atom, that is, the presence of a hydrogen bond with a neutral partner. Considering that  $(^{\text{H}}\text{O})^-$  may exist in solution in both phenol-benzimidazolate and phenolate-benzimidazole forms,<sup>[28]</sup> either a simple ET or an alternative unprecedented PET mechanism may be considered for its one-electron oxidation [Eq. (4)], as in the case of the tyrosinate-histidine pair of PS II suggested by Faller et al. (Figure 1).<sup>[19]</sup>



In summary we have shown that phenoxyl radical properties (oxidation potential, geometric and electronic structures) as well as oxidation mechanism are subtly modulated by the distance/charge of the hydrogen-bonded benzimidazole moiety and thus indirectly by the strength of this hydrogen bond. Furthermore, the correlation observed between the  $g$  tensor and the radical structure is of particular importance in unravelling biological processes involving tyrosyl radicals by HF-EPR, as exemplified by the works of Faller et al. on PSII.

## Experimental Section

**General:** X-Band EPR spectra were recorded on a Bruker ESP 300E spectrometer at 293 K on 50  $\mu$ L samples. Spectra were simulated with the SIMFONIA software (Bruker). High-field EPR spectra were recorded at 285 GHz by using a home made spectrometer (LNCMI, Grenoble, France). NMR spectra were recorded on a Bruker AM 300 ( $^1\text{H}$  at 300 MHz,  $^{13}\text{C}$  at 75 MHz). Chemical shifts are given relative to tetramethylsilane (TMS). Mass spectra were recorded on a Thermofinnigan (EI/DCI) apparatus. Microanalysis was performed by the Service Central d'Analyse du CNRS (Lyon, France). UV/Vis spectra at 298 K were recorded on a Perkin-Elmer Lambda 2 spectrophotometer equipped with a temperature controller unit set at 298 K. The quartz cell path length was 1.000 cm. UV/Vis spectra 238 K were recorded on a Cary 50 spectrophotometer equipped with a Hellma low-temperature immersion probe (1.000 cm path length quartz cell). The temperature was controlled with a Lauda RK8 KS cryostat.

**Electrochemistry:** Cyclic voltammetry curves were recorded on a CHI 660 potentiostat in a standard three-electrode cell under argon atmosphere. An Ag/AgNO<sub>3</sub> (0.01 M) reference electrode was used. All the potentials given in the text are referred to the regular Fe/Fc<sup>+</sup> redox couple used as external reference. A vitreous carbon disc electrode (5 mm diameter) polished with 1  $\mu$ m diamond paste was used as working electrode. Electrolysis was performed on a PAR 273 potentiostat under argon atmosphere at  $-40^\circ\text{C}$  with a carbon-felt working electrode.

**Crystal structure analysis:** For all structures, collected reflections were corrected for Lorentz and polarisation effects but not for absorption. The structures were solved by direct methods and refined with TEXSAN ( $^1\text{H}$ OH,  $^{\text{Me}}\text{OH}$ , ( $^1\text{H}$ O)[ $n\text{Bu}_4\text{N}$ ], ( $^{\text{Me}}\text{O}$ )[ $n\text{Bu}_4\text{N}$ ])<sup>[28]</sup> and OLEX2 software ( $^{\text{pMe}}\text{OH}$ )<sup>[29]</sup>. All non-hydrogen atoms were refined with anisotropic thermal parameters. Hydrogen atoms were generated in idealised positions, riding on the carrier atoms, with isotropic thermal parameters except the hydroxyl ones, which were localised on the Fourier map and fixed. CCDC-236867 ( $^1\text{H}$ OH), CCDC-236868 ( $^{\text{Me}}\text{OH}$ ), CCDC-824137 ( $^1\text{H}$ O)-[ $n\text{Bu}_4\text{N}$ ], CCDC-827959 ( $^{\text{Me}}\text{O}$ )[ $n\text{Bu}_4\text{N}$ ] and CCDC-832162 ( $^{\text{pMe}}\text{OH}$ ) contain the supplementary crystallographic data for this paper. These data can be obtained free of charge from The Cambridge Crystallographic Data Centre via [www.ccdc.cam.ac.uk/data\\_request/cif](http://www.ccdc.cam.ac.uk/data_request/cif).

**Computational details:** Theoretical calculations were based on DFT and were performed with the ORCA program package.<sup>[29]</sup> Geometry optimisations were carried out by using the GGA functional B3LYP<sup>[30–31]</sup> in combination with the TZVP/P<sup>[32]</sup> basis set for all atoms and by taking advantage of the resolution of the identity (RI) approximation in the Split-RI-J variant<sup>[33]</sup> with the appropriate Coulomb fitting sets. Increased integration grids (Grid4 in ORCA convention) and tight SCF convergence criteria were used. For both geometry optimisation and molecular-property calculations, solvent effects were accounted for according to the experimental conditions. For that purpose, we used CH<sub>2</sub>Cl<sub>2</sub> ( $\epsilon = 9.08$ ) as solvent within the framework of the conductor-like screening (COSMO) dielectric continuum approach.<sup>[34]</sup> EPR parameters were obtained from additional single-point calculations with the hybrid functional B3LYP and the EPR-II<sup>[35]</sup> basis set. The  $g$  tensor was calculated as a second derivative property of the energy with respect to the external magnetic field and the electron magnetic moment. For that purpose, the coupled-perturbed Kohn–Sham equations were employed in conjunction with a parametrised one-electron spin–orbit operator.<sup>[36–38]</sup> Hyperfine coupling constants were calculated directly from Fermi contact terms and dipolar contributions as the expectation values of the appropriate operator over the spin density. The spin–orbit contribution (SOC) of the hyperfine interaction was also calculated and its isotropic part was added to the Fermi contact term whereas its anisotropic part was added to the dipolar contribution.<sup>[39]</sup>

**Phenolic compound  $^1\text{H}$ OH** was synthesised as previously reported.<sup>[10]</sup>

**2-(1H-Benzol[d]imidazol-2-yl)-4,6-di-tert-butylphenolate tetrabutylammonium salt ( $^1\text{H}$ O)[ $n\text{Bu}_4\text{N}$ ]:**  $^1\text{H}$ OH (100 mg, 0.31 mmol) was dissolved in Et<sub>2</sub>O (6 cm<sup>3</sup>), after which 1 equiv of NBu<sub>4</sub>OH (310.5  $\mu$ L of a 1 M solution in MeOH) was added, and the reaction mixture was left stirring for 1 h

at room temperature under N<sub>2</sub> atmosphere. The solvent was then removed under vacuum to give an off-white crystalline powder. Colourless block single crystals suitable for X-ray crystallography were obtained by slow evaporation of an Et<sub>2</sub>O solution. Yield: 83%.  $^1\text{H}$  NMR (300 MHz, CDCl<sub>3</sub>):  $\delta$ /ppm = 8.55 (d, 1H, PhOH), 7.58 (m, 2H, Bzim), 7.19 (d, 1H, PhOH), 6.94 (dd, 2H, Bzim), 2.88 (t, 8H, NBu<sub>4</sub>), 1.48 (s, 9H, *t*Bu), 1.34 (s, 9H, *t*Bu), 1.27 (m, 16H, NBu<sub>4</sub>), 0.91 (t, 12H, NBu<sub>4</sub>); MS (ESI(–)):  $m/z$  423 [ $M$ ]<sup>–</sup>; elemental analysis (%) calcd for C<sub>43</sub>H<sub>63</sub>N<sub>5</sub>O·H<sub>2</sub>O: C 75.50, H 9.58, N 10.24, O 4.68; found: C 75.21, H 9.37, N 10.19, O 4.04.

**N-Methyl-2-(2'-hydroxy-3',5'-di-tert-butylphenyl)benzimidazole ( $^{\text{Me}}\text{OH}$ ):** To 3,5-di-tert-butylsalicylaldehyde (411 mg, 1.76 mmol) was added 6 mL of 40% NaHSO<sub>3</sub>(aq). The mixture was stirred for 5 h at 25  $^\circ\text{C}$ . N-Methyl-1,2-phenylenediamine (215 mg, 1.76 mmol) and ethanol (5 mL) were added. The mixture was heated to reflux for 24 h and the reaction mixture was then poured into 150 mL of water. The pale yellow precipitate was filtered off and recrystallised from CH<sub>2</sub>Cl<sub>2</sub>. Yield: 83%. Single crystals were obtained by slow evaporation of a toluene solution.  $^1\text{H}$  NMR (300 MHz, CDCl<sub>3</sub>):  $\delta$ /ppm = 12.48 (s, 1H, OH), 7.75 (m, 1H, Bzim), 7.50 (d, 1H, PhOH), 7.44 (d, 1H, PhOH), 7.42 (m, 1H, Bzim), 7.34 (m, 2H, Bzim), 4.03 (s, 3H, CH<sub>3</sub>), 1.49 (s, 9H, *t*Bu), 1.37 (s, 9H, *t*Bu); MS (DCI, NH<sub>3</sub>/isobutane):  $m/z$  337 [ $M+\text{H}$ ]<sup>+</sup>; elemental analysis (%) calcd for C<sub>22</sub>H<sub>28</sub>N<sub>2</sub>O: C 78.53, H 8.39, N 8.33; found: C 78.32, H 8.27, N 8.27.

**2,4-Di-tert-butyl-6-(1-methyl-1H-benzol[d]imidazol-2-yl)phenolate tetrabutylammonium salt ( $^{\text{Me}}\text{O}$ )[ $n\text{Bu}_4\text{N}$ ]:**  $^{\text{Me}}\text{OH}$  (50 mg, 0.15 mmol) was dissolved in Et<sub>2</sub>O (6 cm<sup>3</sup>), after which 1 equiv of NBu<sub>4</sub>OH (155  $\mu$ L of a 1 M solution in MeOH) was added, and the reaction mixture was left stirring for 1 h at room temperature under N<sub>2</sub> atmosphere. The solvent was then removed under vacuum yielding a brown oily material, which was washed several times with pentane to give light yellow-green solid. Yield: 86%. Yellowish block single crystals suitable for X-ray crystallography were obtained by slow evaporation of a pentane solution.  $^1\text{H}$  NMR (200 MHz, CDCl<sub>3</sub>):  $\delta$ /ppm = 7.75 (m, 1H, Bzim), 7.49 (s, 1H, PhOH), 7.44 (s, 1H, PhOH), 7.40 (s, 1H, Bzim), 7.35 (m, 2H, Bzim), 4.02 (s, 3H, CH<sub>3</sub>), 3.38 (t, 8H, NBu<sub>4</sub>), 1.64 (m, 8H, NBu<sub>4</sub>), 1.49 (s, 9H, *t*Bu), 1.36 (s, 9H, *t*Bu), 1.39 (m, 8H, NBu<sub>4</sub>), 0.97 (t, 12H, NBu<sub>4</sub>); MS (ESI(–)):  $m/z$  423 [ $M$ ]<sup>–</sup>; elemental analysis (%) calcd for C<sub>43</sub>H<sub>63</sub>N<sub>5</sub>O·H<sub>2</sub>O: C 75.50, H 9.58, N 10.24, O 4.68; found: C 75.21, H 9.37, N 10.19, O 4.04%.

**N-Methyl-2-(4'-hydroxy-3',5'-di-tert-butylphenyl)benzimidazole ( $^{\text{pMe}}\text{OH}$ ):** HL<sup>pMe</sup> was prepared in a similar way to HL<sup>Me</sup> from 3,5-di-tert-butyl-4-hydroxybenzaldehyde and N-methyl-1,2-phenylenediamine. Single crystals were grown by slow evaporation of a concentrated CH<sub>2</sub>Cl<sub>2</sub>:toluene (1:5) solution. Yield: 91%.  $^1\text{H}$  NMR (300 MHz, DMSO):  $\delta$  1.46 (18H, s), 3.87 (3H, s), 7.28–7.18 (2H, m), 7.57–7.54 (3H, m), 7.70 (1H, d); MS (DCI, NH<sub>3</sub>/isobutane):  $m/z$  337 [ $M+\text{H}$ ]<sup>+</sup>; elemental analysis (%) calcd for C<sub>22</sub>H<sub>28</sub>N<sub>2</sub>O: C 78.53, H 8.39, N 8.33; found: C 78.42, H 8.22, N 8.19.

- [1] J. Stubbe, W. A. Van der Donk, *Chem. Rev.* **1998**, 98, 705; J. Stubbe, D. G. Nocera, C. S. Yee, M. C. Y. Chang, *Chem. Rev.* **2003**, 103, 2167.
- [2] D. A. Force, D. W. Randall, R. D. Britt, X. S. Tang, B. A. Diner, *J. Am. Chem. Soc.* **1995**, 117, 12643; M. T. Bernard, G. M. Macdonald, A. P. Nguyen, R. J. Debus, B. A. Barry, *J. Biol. Chem.* **1995**, 270, 1589; S. Un, X. S. Tang, B. A. Diner, *Biochemistry* **1996**, 35, 679; X. S. Tang, M. Zheng, D. A. Chisholm, G. C. Dismukes, B. A. Diner, *Biochemistry* **1996**, 35, 1475; B. A. Diner, D. A. Force, D. W. Randall, R. D. Britt, *Biochemistry* **1998**, 37, 17931; P. Dorlet, W. Rutherford, S. Un, *Biochemistry* **2000**, 39, 7826; B. A. Diner, *Biochim. Biophys. Acta Bioenerg.* **2001**, 1503, 147; R. J. Debus, *Biochim. Biophys. Acta Bioenerg.* **2001**, 1503, 164.
- [3] S. Un, M. Atta, M. Fontecave, A. W. Rutherford, *J. Am. Chem. Soc.* **1995**, 117, 10713.
- [4] N. Ito, S. E. V. Phillips, C. Stevens, Z. B. Ogel, M. J. McPherson, J. N. Keen, K. D. S. Yadav, P. J. Knowles, *Nature* **1991**, 350, 87; G. T. Babcock, M. K. El-Deeb, P. O. Sandusky, M. M. Whittaker, J. W. Whittaker, *J. Am. Chem. Soc.* **1992**, 114, 3727; N. Ito, S. E. V. Phillips, K. D. S. Yadav, P. F. Knowles, *J. Mol. Biol.* **1994**, 238, 704; J. W. Whittaker, in *Advances in Protein Chemistry*, Vol. 60 (Eds.: F. M. Ri-

- chards, D. S. Eisenberg, J. Kuriyan), Academic Press, Elsevier, **2002**, pp. 1–49; J. W. Whittaker, *Chem. Rev.* **2003**, *103*, 2347; M. S. Rogers, D. M. Dooley, *Curr. Opin. Chem. Biol.* **2003**, *7*, 189; F. Thomas, *Eur. J. Inorg. Chem.* **2007**, 2379.
- [5] P. P. Schmidt, K. K. Andersson, A. L. Barra, L. Thelander, A. Graslund, *J. Biol. Chem.* **1996**, *271*, 9809; P. J. Van Dam, J. P. Willems, P. P. Schmidt, S. Pötsch, A. L. Barra, W. R. Hagen, B. M. Hoffman, K. K. Andersson, A. Graslund, *J. Am. Chem. Soc.* **1998**, *120*, 5080.
- [6] C. J. Chang, M. C. Y. Chang, N. H. Damrauer, D. G. Nocera, *Biochim. Biophys. Acta Bioenerg.* **2004**, 1655, 13.
- [7] P. Dorlet, S. A. Seibold, G. T. Babcock, G. J. Gerfen, W. L. Smith, A. L. Tsai, S. Un, *Biochemistry* **2002**, *41*, 6107.
- [8] T. Maki, Y. Araki, Y. Ishida, O. Onomura, Y. Matsumura, *J. Am. Chem. Soc.* **2001**, *123*, 3371.
- [9] F. Thomas, O. Jarjays, C. Duboc, C. Philouze, E. Saint-Aman, J.-L. Pierre, *Dalton Trans.* **2004**, 2662.
- [10] L. Benisvy, R. Bittl, E. Bothe, C. D. Garner, J. McMaster, S. Ross, C. Teutloff, F. Neese, *Angew. Chem.* **2005**, *117*, 5448; *Angew. Chem. Int. Ed.* **2005**, *44*, 5314; L. Benisvy, E. Bill, A. J. Blake, D. Collison, E. S. Davies, C. D. Garner, G. McArdle, E. J. L. McInnes, J. McMaster, S. H. K. Rossa, C. Wilson, *Dalton Trans.* **2006**, 258.
- [11] C. Costentin, M. Robert, J. M. Savéant, *J. Am. Chem. Soc.* **2006**, *128*, 8726; C. Costentin, M. Robert, J. M. Savéant, *J. Am. Chem. Soc.* **2006**, *128*, 4552; I. J. Rhile, T. F. Markle, H. Nagao, A. G. DiPasquale, O. P. Lam, M. A. Lockwood, K. Rotter, J. M. Mayer, *J. Am. Chem. Soc.* **2006**, *128*, 6075.
- [12] T. F. Markle, I. J. Rhile, A. G. DiPasquale, J. M. Mayer, *Proc. Natl. Acad. Sci. USA* **2008**, *105*, 8185.
- [13] L. Benisvy, D. Hammond, D.-J. Parker, E.-S. Davies, C.-D. Garner, J. McMaster, C. Wilson, F. Neese, E. Bothe, R. Bittl, C. Teutloff, *J. Inorg. Biochem.* **2007**, *101*, 1859.
- [14] R. Wanke, L. Benisvy, M. L. Kuznetsov, M. F. C. Guedes da Silva, A. J. L. Pombeiro, *Chem. Eur. J.* **2011**, *17*, 11882.
- [15] F. Lachaud, A. Quaranta, Y. Pellegrin, P. Dorlet, M. F. Charlot, S. Un, W. Leibl, A. Aukauloo, *Angew. Chem.* **2005**, *117*, 1560; *Angew. Chem. Int. Ed.* **2005**, *44*, 1536; G. F. Moore, M. Hambourger, M. Gervaldo, O. G. Poluektov, T. Rajh, D. Gust, T. A. Moore, A. L. Moore, *J. Am. Chem. Soc.* **2008**, *130*, 10466.
- [16] G. F. Moore, M. Hambourger, G. Kodis, W. Michl, D. Gust, T. A. Moore, A. L. Moore, *J. Phys. Chem. B* **2010**, *114*, 14450.
- [17] F. Thomas, O. Jarjays, H. Jamet, S. Hamman, E. Saint-Aman, C. Duboc, J. L. Pierre, *Angew. Chem.* **2004**, *116*, 604; *Angew. Chem. Int. Ed.* **2004**, *43*, 594.
- [18] C. Costentin, M. Robert, J.-M. Savéant, *Chem. Rev.* **2010**, *110*, PR1.
- [19] P. Faller, C. Goussias, A. W. Rutherford, S. Un, *Proc. Natl. Acad. Sci. USA* **2003**, *100*, 8732.
- [20] a) P. George, G. I. H. Hanania, D. H. Irvine, I. Abu-Issa, *J. Chem. Soc.* **1964**, 5689; b) P. M. A. Gadsby, A. J. Thomson, *FEBS Lett.* **1982**, *150*, 59.
- [21] F. Michel, F. Thomas, S. Hamman, C. Philouze, E. Saint-Aman, J. L. Pierre, *Eur. J. Inorg. Chem.* **2006**, 3684.
- [22] R. Liu, K. Morokuma, A. M. Mebel, M. C. Lin, *J. Phys. Chem.* **1996**, *100*, 9314; A. Hinchliffe, R. E. Steinbank, M. A. Ali, *Theor. Chim. Acta* **1966**, *5*, 95; H. M. Chang, H. H. Jaffe, *Chem. Phys. Lett.* **1973**, *23*, 146; H. M. Chang, H. H. Jaffe, C. A. Masmandis, *J. Phys. Chem.* **1975**, *79*, 1118; J. Takahashi, T. Shida, *Bull. Chem. Soc. Jpn.* **1994**, *67*, 2038; J. Takahashi, T. Momose, T. Shida, *Bull. Chem. Soc. Jpn.* **1994**, *67*, 964; L. J. Johnston, N. Mathivanan, F. Negri, W. Siebrand, F. Zerbetto, *Can. J. Chem.* **1993**, *71*, 1655; J. G. Radziszewski, M. Gil, A. Gorski, J. Spanget-Larsen, J. Waluk, B. J. Mroz, *J. Chem. Phys.* **2001**, *115*, 9733.
- [23] C. Xie, P. M. Lahti, *Tetrahedron Lett.* **1999**, *40*, 4305.
- [24] The calculated hyperfine coupling constants for the other compounds are given in the Supporting Information. From these calculated values the most expanded spectrum is expected to be that of (pMeO)<sup>•</sup>, as experimentally observed.
- [25] a) A. Sokolowski, E. Bothe, E. Bill, T. Weyhermüller, K. Wieghardt, *Chem. Commun.* **1996**, 1671; b) L. Benisvy, A. J. Blake, D. Collison, E. S. Davies, C. D. Garner, E. J. L. McInnes, J. McMaster, G. Whittaker, C. Wilson, *Chem. Commun.* **2001**, 1824; c) L. Benisvy, A. J. Blake, D. Collison, E. S. Davies, C. D. Garner, E. J. L. McInnes, J. McMaster, G. Whittaker, C. Wilson, *Dalton Trans.* **2003**, 1975; d) V. W. Manner, T. F. Markle, J. H. Freudenthal, J. P. Roth, J. M. Mayer, *Chem. Commun.* **2008**, 256; e) Y. Shimazaki, T. D. P. Stack, T. Storr, *Inorg. Chem.* **2009**, *48*, 8383; f) T. Storr, P. Verma, Y. Shimazaki, E. C. Wasinger, T. D. P. Stack, *Chem. Eur. J.* **2010**, *16*, 8980; g) M. Orto, O. Jarjays, H. Kano, C. Philouze, F. Neese, F. Thomas, *Angew. Chem.* **2010**, *122*, 5109; *Angew. Chem. Int. Ed.* **2010**, *49*, 4989; h) Y. Shimazaki, N. Arai, T. J. Dunn, T. Yajima, F. Tani, C. F. Ramogida, T. Storr, *Dalton Trans.* **2011**, *40*, 2469.
- [26] P. J. O'Malley, *J. Am. Chem. Soc.* **1998**, *120*, 11732.
- [27] E. L. Fasanella, W. Gordy, *Proc. Natl. Acad. Sci. USA* **1969**, *62*, 299; A. L. Maniero, V. Chis, A. Zoleo, M. Brustolon, A. Mezzetti, *J. Phys. Chem. B* **2008**, *112*, 3812.
- [28] B. H. Robinson, in *Proton-Transfer Reactions* (Eds.: E. Caldin, V. Gold), Chapman and Hall, London, **1975**, pp. 121–152.
- [29] F. Neese, ORCA—an ab initio, Density Functional and Semiempirical Program Package (v. 2.8), Universität Bonn, Bonn (Germany), **2007**.
- [30] A. D. Becke, *J. Chem. Phys.* **1993**, *98*, 5648.
- [31] C. Lee, W. Yang, R. G. Parr, *Phys. Rev. B* **1988**, *37*, 785.
- [32] A. Schäfer, C. Huber, R. J. Ahlrichs, *J. Chem. Phys.* **1994**, *100*, 5829.
- [33] A. Weigend, *Phys. Chem. Chem. Phys.* **2006**, *8*, 1057.
- [34] A. Klamt, G. Schürmann, *J. Chem. Soc. Perkin Trans. 2* **1993**, 793.
- [35] V. Barone, *Recent Advances in Density Functional Methods, Part 1* (Ed.: D. P. Chong) World Scientific, Singapore, **1996**.
- [36] F. Neese, *J. Chem. Phys.* **2001**, *115*, 11080.
- [37] S. Koseki, M. W. Schmidt, M. S. Gordon, *J. Phys. Chem.* **1992**, *96*, 10768; M. S. Gordon, *J. Phys. Chem.* **1992**, *96*, 10768.
- [38] S. Koseki, M. S. Gordon, M. W. Schmidt, N. Matsunaga, *J. Phys. Chem.* **1995**, *99*, 12764.
- [39] F. Neese, *J. Chem. Phys.* **2003**, *118*, 3939.

Received: September 13, 2011  
Published online: March 13, 2012